Characterizing a role for α-parvin in *Xenopus laevis* Development

by

Richard Do

A thesis
presented to the University of Waterloo
in fulfillment of the
thesis requirement for the degree of
Master of Science
in
Biology

Waterloo, Ontario, Canada, 2021

AUTHOR'S DECLARATION

I hereby declare that I am the sole author of this thesis. This is a true copy of the thesis, including any required final revisions, as accepted by my examiners.

I understand that my thesis may be made electronically available to the public.

Abstract

In metazoans dynamic regulation of cell adhesion is critical for the cell movements that characterize gastrulation. It is clear that the adhesive property of cells is modulated in a highly coordinated spatial and temporal fashion. In *Xenopus,* gastrulation has been extensively characterized at the cell and tissue level. The directed intercalation of cells generates the forces that drive tissue shape changes and rearrangements. In *Xenopus,* the adhesive properties of cells are mediated through the integrin and cadherin families of cell adhesion receptors. The integrins mediate bidirectional signaling across cell membranes. Integrin ligation recruits multi-protein complexes such as the ILK-PINCH-Parvin (IPP) complex to the cytoplasmic tail at sites of focal adhesion. α-parvin is a member of the IPP complex and has two functional calponin-homology (CH) domains. In the IPP complex, α-parvin primarily functions as a scaffolding molecule. However, the mechanistic role of α-parvin has yet to be described in *Xenopus*. I asked if α-parvin acts as an active modulator of integrin-mediated adhesion during *Xenopus laevis* gastrulation.

I successfully isolated *Xenopus* α-parvin and performed a phylogenetic analysis on the sequence. α-parvin shares high sequence identity with α-parvin orthologs from other model organisms. The CH domains are also highly conserved. *Xenopus* α-parvin displays peak expression levels during gastrulation suggesting a role in the rearrangement of cells and tissues during gastrulation. To analyze function, I created GFP tagged α-parvin deletion constructs that isolate each domain. In *Xenopus* A6 cells, the full length α-parvin construct localizes to focal adhesions. The isolated CH1 domain is not recruited to focal adhesions, while the isolated CH2 domain is found in focal adhesions. This suggests that the CH2

domain of *Xenopus* α-parvin is responsible for recruitment to sites of integrin adhesion. In embryos, over-expression of full length α-parvin has no effect on development. When the CH1 domain is over expressed, blastopore closure is delayed and anterior–posterior axis extension is inhibited. These embryos develop axial protrusions that resemble a second axis. This would suggest that the CH1 domain is somehow influencing the β-catenin pathway that influences axial development. When the CH2 domain is over expressed, embryos show a dramatic delay and failure of blastopore closure. The anterior-posterior axis is truncated, and the blastocoel is retained. The embryos over-expressing the CH2 domain resemble those in which integrin-FN interactions are disrupted and it is likely that the CH2 domain is acting as a dominant negative to inhibit integrin adhesion. This thesis provides a preliminary analysis of α-parvin function in *Xenopus laevis* development.

Acknowledgments

I feel very fortunate to have Dr. Mungo Marsden as my supervisor. He was kind, supportive, patient, and most of all, truly invested in my success. What more could you ask for from a mentor? I thank him for being a great role model, and for his guidance during the course of my graduate studies.

I would like to thank the members of my committee Dr. Bruce Reed and Dr. Dale Martin for their valuable insight.

I want to thank my great friends, Jotham Candido and Jerusha Rupakumar. I have shared much of the journey of life with them, and they have made it infinitely more enjoyable.

I am very appreciative of my family for their never-ending support. Without my parents and sister, I would never be the person I am today.

Finally, I want to express my love and gratitude to Vivian Chan. Thank you for all the laughs and memories over the years. Thank you for your comforting words and support during the hard times and thank you for your smiles and companionship through the good times.

Table of Contents

AUTHOR'S DECLARATION ii
Abstract iii
Acknowledgments v
List of Figures viii
List of Tables ix
List of Abbreviations x
1.0 Introduction 1
1.1 *Xenopus* Gastrulation 1
1.2 Cell Adhesion Receptors 6
1.3 Integrin-Mediated Adhesion in *Xenopus* 8
1.4 IPP Complex 10
1.4.1 ILK 11
1.4.2 PINCH 12
1.5 Parvin 13
1.5.1 β-parvin 14
1.5.2 α-parvin 14
1.5.3 Antagonistic relationship between α-parvin and β-parvin 15
1.6 β-parvin in *Xenopus* 16
1.7 Summary 18
2.0 Materials and Methods 19
2.1 Cloning α-parvin 19
2.1.1 Isolation of a cDNA representing *Xenopus* α-parvin 19
2.1.2 Isolation of cDNA representing α-parvin 21
2.1.3 Sub-cloning α-parvin 22
2.1.4 α-parvin Deletion Constructs 23
2.1.5 GFP Fusion Constructs 24
2.2 *in vitro* mRNA Transcription 25
2.3 Tissue Culture 26
2.3.1 Maintenance of *Xenopus* A6 Cells 26
2.3.2 Transfection of *Xenopus* A6 Cells 26

2.4 Maintenance and Manipulations of *Xenopus laevis* Embryos 27
2.5 Embryo Microinjections 28
2.5.1 Imaging 28
2.6 Western blotting 28
3.0 Results 30
3.1 Isolation of *Xenopus laevis* α-parvin 30
3.2 Phylogenetic Analysis of *Xenopus* α-parvin 32
3.3 Temporal Expression of *Xenopus* α-parvin 36
3.4 α-parvin is recruited to sites of focal adhesion 38
3.4.1 Expression of Fusion Constructs 38
3.4.2 Localization of GFP-α-parvin in *Xenopus* A6 cells 40
3.4.3 Co-localization of GFP-α-parvin and RFP-β-parvin in *Xenopus* A6 cells 41
3.5 A role for α-parvin in embryonic development 45
3.5.1 CH1 and CH2 delay blastopore closure 48
3.5.2 CH1 and CH2 domains of α-parvin interfere with tissue rearrangements during gastrulation 54
3.5.3 CH1 and CH2 disrupt the anterior-posterior axis 60
3.5.4 Tadpoles exhibit downstream defects of CH1 and CH2 disruption during gastrulation 66
4.0 Discussion 70
4.1 Cloning and sequence analysis of *Xenopus* α-parvin 70
4.2 α-parvin expression is increased during gastrulation 73
4.3 α-parvin and CH2 compartmentalize to focal adhesions *in vitro* 74
4.4 Functional analysis of α-parvin CH domains during *Xenopus* embryogenesis 77
4.4.1 The isolated CH1 domain of α-parvin causes developmental defects 78
4.4.2 The CH2 domain of α-parvin affects integrin adhesion 79
4.5 Conclusion 81
4.6 Future Directions 81
References 83

List of Figures

Figure 1.1 *Xenopus laevis* embryo development. 3
Figure 1.2 Cell intercalation and tissue movements during gastrulation. 5
Figure 1.3 The integrin superfamily 9
Figure 1.4 The ILK-PINCH-Parvin (IPP) complex and their domains 10
Figure 2.2 α-parvin RP1 and RP2 deletion constructs blueprint 23
Figure 3.1 *Xenopus laevis* α-parvin RT-PCR 31
Figure 3.2 *Xenopus laevis* α-parvin is highly conserved 34
Figure 3.3 *Xenopus* α-parvin clusters with other α-parvins 35
Figure 3.4 α-parvin mRNA is expressed throughout early *Xenopus* embryo development. 37
Figure 3.5 GFP-tagged constructs are expressed as fusion proteins in embryos 39
Figure 3.6 α-parvin and RP2 compartmentalize to focal adhesions in *Xenopus* tissue culture cells 43
Figure 3.7 α-parvin and β-parvin partially co-localize to focal adhesions in *Xenopus* tissue culture cells 44
Figure 3.8 Over-expression of RP1 and RP2 functional domains cause defects 47
Figure 3.9 Overexpression of GFP tag and full-length α-parvin does not delay blastopore closure during *Xenopus* gastrulation 51
Figure 3.10 Over-expression of RP1 and RP2 delays blastopore closure during *Xenopus* gastrulation 53
Figure 3.11 Overexpression of GFP and full-length α-parvin does not inhibit mesoderm extension during gastrulation 57
Figure 3.12 Overexpression of RP1 and RP2 inhibits mesoderm extension during gastrulation 59
Figure 3.13 Overexpression of GFP and full-length α-parvin does not disrupt the anterior-posterior axis 63
Figure 3.14 Overexpression of RP1 and RP2 disrupts the anterior-posterior axis 65
Figure 3.15 Overexpression of GFP and full-length α-parvin does not cause major defects at organogenesis 68
Figure 3.16 Overexpression of RP1 and RP2 cause major defects at organogenesis 69

List of Tables

Table 2.1 PCR primers used to isolate α-parvin, RP1, and RP2 sequences 20

List of Abbreviations

ANK	ankyrin
ATCC	American Type Culture Collection
BS	Bluescript
BSA	bovine serum albumin
DMZ	dorsal marginal zone
CH	calponin homology
CHO	Chinese hamster ovary
EDTA	ethylenediaminetetraacetic acid
ESB	embryo solubilization buffer
F-actin	filamentous actin
FBS	fetal bovine serum
FLAP	full length α-parvin
FN	fibronectin
GFP	green florescence protein
Grb-4	growth factor receptor-bound protein-4
hCG	human chorionic gonadotropin
HEPES	4-(2-hydroxyethyl)-1-piperazineethanesulfonic acid
HRP	horseradish peroxidase
ILK	integrin linked kinase
IPP	ILK-PINCH-parvin
L-15	Leibowitz-15
LB	Luria broth
LIM	Lin-11, Isl-1, Mec-3
MBS	modified Barth's saline
PBS	phosphate buffered saline
PCR	polymerase chain reaction
PDGF	platelet derived growth factor
PH	pleckstrin homology
PINCH	Particularly Interesting New Cysteine-Histidine rich protein
PMSF	phenylmethane sulfonyl fluoride

RFP	Red Fluorescent Protein
RT-PCR	reverse transcription-PCR
SDS	sodium dodecyl sulfate
SDS-PAGE	sodium dodecyl sulfate-polyacrylamide gel electrophoresis
TBS	tris buffered saline
TCA	trichloroacetic acid
TGF-β	transforming growth factor-beta

1.0 Introduction

1.1 *Xenopus* Gastrulation

Xenopus laevis embryos are a widely used model to study molecular processes involved in early development. The site of sperm entry is restricted to the animal hemisphere and determines the future ventral side of the embryo. Fertilization is followed by rotation of the cortical cytoplasm, placing β-catenin on the future dorsal side, opposite the site of sperm entry (Figure 1.1). Following this, a series of rapid cell divisions occurs until a blastula is formed. The end of cleavage is signaled by a slowing and cessation of rapid cell cycles and the embryo forms a hollow sphere. The blastocoel is a fluid filled cavity that lies in the animal half of the blastula, while the yolk mass remains in the vegetal half (Figure 1.1).

In metazoans, gastrulation is a highly conserved stage of embryonic development where the hollow blastula undergoes cell rearrangements to reorganize into a multi-layered gastrula (Muhr & Ackerman, 2021). *Xenopus laevis* is a triploblastic organism, and gastrulation rearranges the three primary germ layers: the ectoderm, mesoderm, and endoderm into the adult body plan. In *Xenopus* the onset of gastrulation is marked by the formation of pigmented bottle cells. Bottle cells are formed from superficial epithelial cells at the site of blastopore formation, (Hardin & Keller, 1988). The apices of the cells constrict while elongating horizontally into the embryo. This area is known as the dorsal lip of the blastopore. The region defined by the bottle cells eventually invaginates into the embryo to form the blastoporal groove (Hardin & Keller, 1988). Following bottle cell formation, the first gross tissue movement observed is vegetal rotation where the yolky vegetal tissue

rotates towards the dorsal side of the embryo resulting in the blastocoel floor moving towards the animal pole. This movement draws cells from the dorsal marginal zone (DMZ) which lies just above the bottle cells into the interior of the embryo (Winklbauer & Schurfeld, 1999). This initial tissue movement also positions the leading-edge mesoderm next to the blastocoel roof.

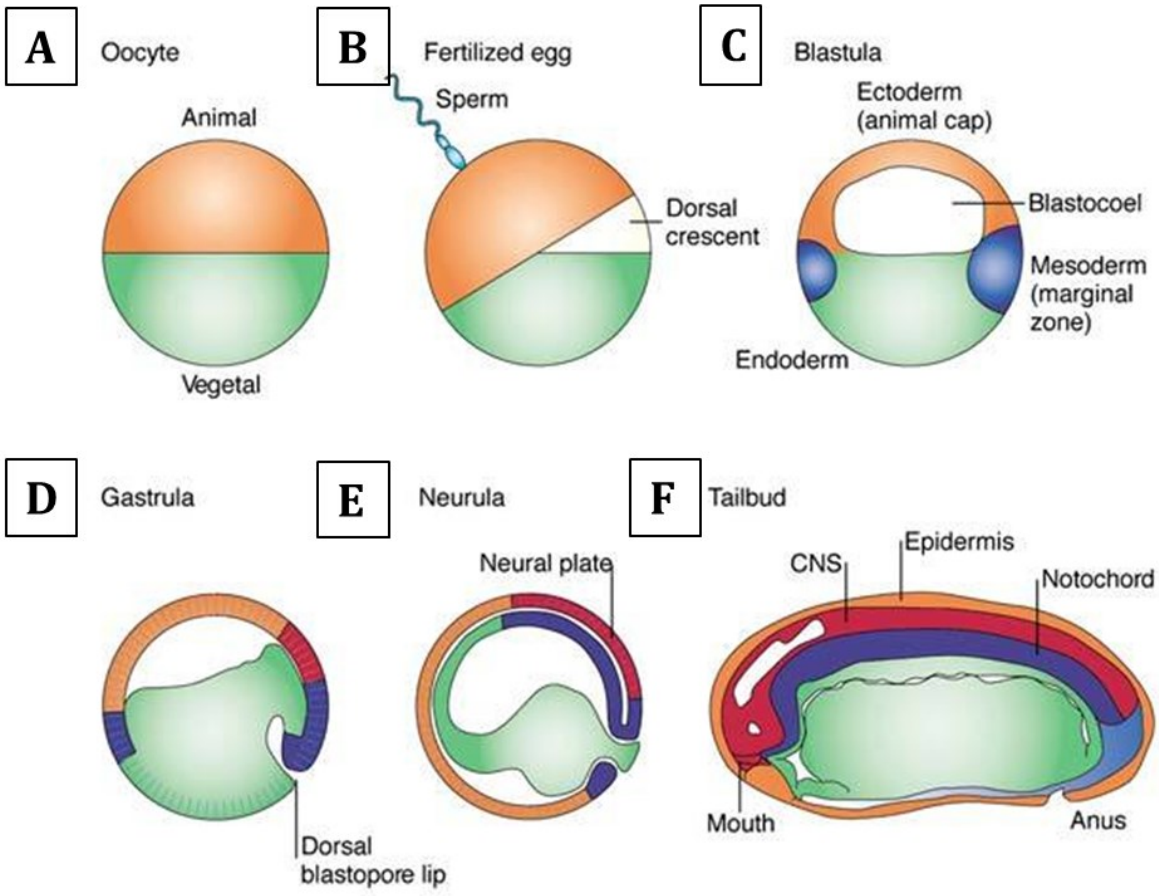

Figure 1.1 *Xenopus laevis* embryo development. Illustration depicting several important developmental milestones in *Xenopus* embryos. The oocyte (A) consists of the animal and vegetal poles. Fertilization in the animal cap is followed by cortical rotation, creating the dorsal crescent (B). The hollow blastula is formed from rapid reductive cleavage cycles in the embryo (C). The fluid filled blastocoel lies in the animal half and the three primary germ layers; mesoderm, endoderm, and ectoderm, are present. Gastrulation (D) rearranges the primary germ layers, beginning with involution of the mesoderm at the dorsal blastopore lip. Following gastrulation, the embryo develops into a neurula (E) where the underlying mesoderm influences the overlying mesoderm to form the neural plate. The embryo then extends in the anterior-posterior axis as it develops into a tadpole (F). At this stage, several organs begin to form, including the central nervous system (CNS), epidermis, notochord, mouth, and anus. (Adapted from Singhal, 2005)

In the animal cap, ectoderm cells undergo radial intercalation (Figure 1.2), reducing the number of layers, thinning, and expanding the blastocoel roof through a movement known as epiboly. Cells on the dorsal side undergo further intercalation in the medial lateral direction (convergent extension) extending this future axial tissue (Figure 1.2). These cell movements push the superficial tissue towards the vegetal pole and consequently actively contributes to involution of the DMZ (Figure 1.2). Marginal zone involution progresses laterally and ventrally during gastrulation, turning the dorsal lip into a ring-shaped blastopore. Epiboly combined with convergent extension eventually closes the blastopore near the end of gastrulation (Wacker et al., 2000).

Superficial mesoderm that surrounds the blastopore involutes into the interior of the embryo. On the dorsal side of the embryo, the radial and subsequent medial lateral intercalation of cells results in convergent extension. Further convergent extension occurs in the mesoderm post-involution extending the axial mesoderm. The medio-lateral convergence of this tissue extends the anterior-posterior axis. This extension drives the anterior mesendoderm across the blastocoel roof towards the anterior of the embryo (Wacker et al., 2000).

Despite the complexity of these tissue rearrangements, it appears that the simple directional intercalation of cells is responsible for the dramatic changes in embryonic form during gastrulation. Both epiboly and convergent extension are driven by local cell movement, and it is the summation of these that drive the dramatic rearrangements that define gastrulation.

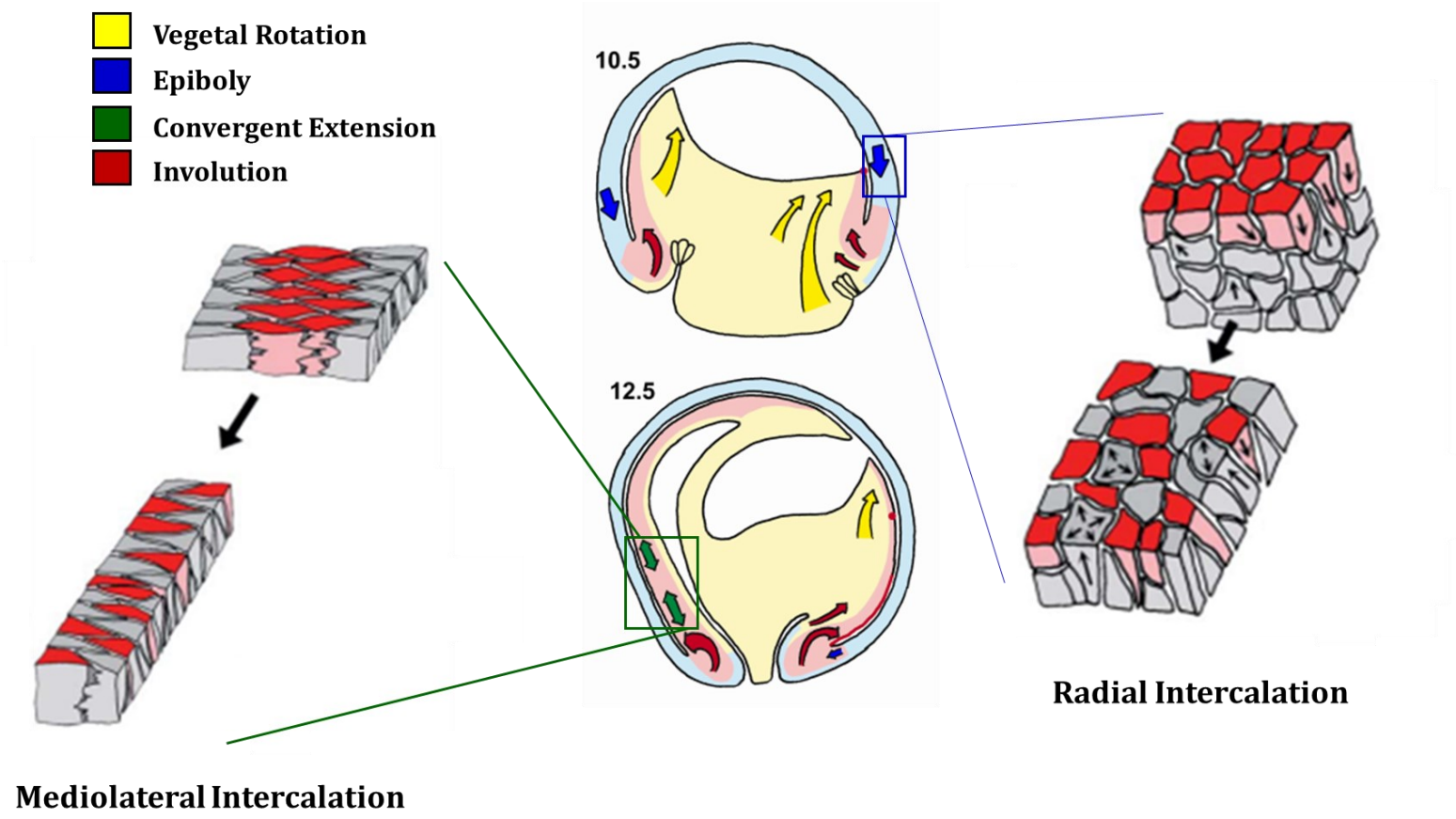

Figure 1.2 Cell intercalation and tissue movements during gastrulation. During gastrulation, the *Xenopus* embryo undergoes extensive tissue rearrangements. Epiboly (blue arrows) is driven by radial intercalation of cells and spreads the superficial epithelium in the ectoderm (blue) ventrally towards the blastopore lip. Vegetal rotation (yellow arrows) passively draws the endoderm (yellow) towards the animal pole, promoting involution (red arrows) and positioning the mesoderm next to the blastocoel roof (red). Convergent extension (green) is driven by mediolateral intercalation and is a driving force for mesoderm attachment and extension across the blastocoel roof. (Adapted from Keller et al., 2003)

1.2 Cell Adhesion Receptors

The tissue rearrangements during gastrulation, described above, are dependent on a small number of cell adhesion receptors (Kraft et al., 2012). Cell adhesion in early *Xenopus laevis* embryos is modulated primarily by two families of trans-membrane receptors: cadherins and integrins. The cadherin family of receptors modulates physical interactions between cells while integrins mediate interactions between cells and the extra-cellular matrix.

Cadherins are a large and diverse super family of transmembrane receptors. They normally consist of homodimers that interact with similar receptors in neighboring cells. In the early gastrula stage embryo, two cadherins are present (Detrick et al., 1990; Ginsberg et al., 1991). E-cadherin is restricted to the superficial ectoderm and is responsible for epidermal integrity. C-cadherin has a more ubiquitous expression (Levi et al., 1991) and modulation of its affinity is crucial to proper tissue movements during gastrulation (Levi et al., 2001; Lee & Gumbiner, 1995). The roles that C-cadherin play in gastrulation are both direct and indirect. An increase in C-cadherin adhesion creates tension across the blastocoel roof, which is necessary for fibronectin (FN) matrix assembly on the free surface (Dzamba et al., 2009). At the dorsal lip, post-involution mesoderm receives signals that result in an affinity modulation of C-cadherin that allows for cell intercalation (Brieher & Gumbiner, 1994).

Cadherin dimer formation at sites of cell-cell adhesion initiates recruitment of several molecules to the cytoplasmic tail, such as β-catenin and plakoglobin (Kraft et al., 2012; Gumbiner, 2000). Both molecules mediate the interaction between cadherins and the

actin cytoskeleton, (McCrea & Gottardi, 2016) while plakoglobin can also facilitate interactions between cadherins and intermediate filaments (Leonard et al., 2008). β-catenin is essential for actin recruitments to sites of cadherin adhesion (McCrea & Gottardi, 2015), and is also a key member in the canonical Wnt signaling pathway (reviewed in Gumbiner, 2005). β-catenin plays many roles in this pathway including indirect modulation of the actin cytoskeleton through α-catenin and associating with transcription factors to transcribe Wnt/β-catenin genes in the nucleus. Free β-catenin is usually targeted for degradation by a destruction complex (reviewed in Fagotto, 2013). In *Xenopus*, β-catenin is protected from destruction and accumulates in the dorsal side of the post-fertilization embryo (Schneider et al., 1996) where it induces the formation of the dorso-anterior axis (Schneider et al., 1996).

Integrins mediate interactions between the cell and its immediate environment. Functional integrin receptors are transmembrane heterodimers formed by the association of alpha and beta subunits. Mammals display the most complex array of integrin subunits. There are 18 α-subunits and eight β-subunits (Figure 1.3). Together, they form 24 integrin receptors, each interacting with a unique ligand (reviewed in Takada et al., 2007). Once the extracellular domain binds a ligand, the cytoplasmic tail undergoes a conformation change and actively recruits cytoplasmic protein complexes. In tissue culture cells these sites are known as focal adhesions and contain over 180 different molecules with over 700 predicted protein interactions (Zaidel-Bar and Geiger, 2010). Integrin signaling mediates a number of cellular functions such as cell migration, proliferation, survival, as well as tissue morphogenesis.

1.3 Integrin-Mediated Adhesion in *Xenopus*

During early *Xenopus laevis* development, three integrins are expressed, αVβ3, α3β1 and α5β1 (Figure 1.3). α5β1 integrin is the only functional receptor and is ubiquitously expressed (Hoffstrom, 2002). During the blastula stage, all cells express α5β1 integrin and secrete soluble FN (Lee et al., 1984), but matrix assembly only occurs on the free surface of the blastocoel roof, implying spatial modulation of adhesive properties (Lee et al., 1984). FN fibrillogenesis begins when α5β1 integrin binds to soluble FN. This is followed by increased C-cadherin surface expression and cell-cell adhesion. The increase in cadherin adhesion results in F-actin accumulation and myosin-light chain II phosphorylation generates tension along the blastocoel roof which is transmitted to the bound FN through α5β1. The tension causes bound FN to unfold and promotes self-assembly of a matrix. Once the FN matrix is formed, α5β1 integrin transmits a signal causing decreased tension in C-cadherin junctions, allowing the intercalation and rearrangement of cells (Marsden and DeSimone, 2003). In summary, α5β1-FN ligation is necessary for both FN matrix assembly and indirectly in the intercalation of cells involved in convergent extension and epiboly (Davidson et al., 2006; Marsden & DeSimone, 2001; Rozario et al., 2009).

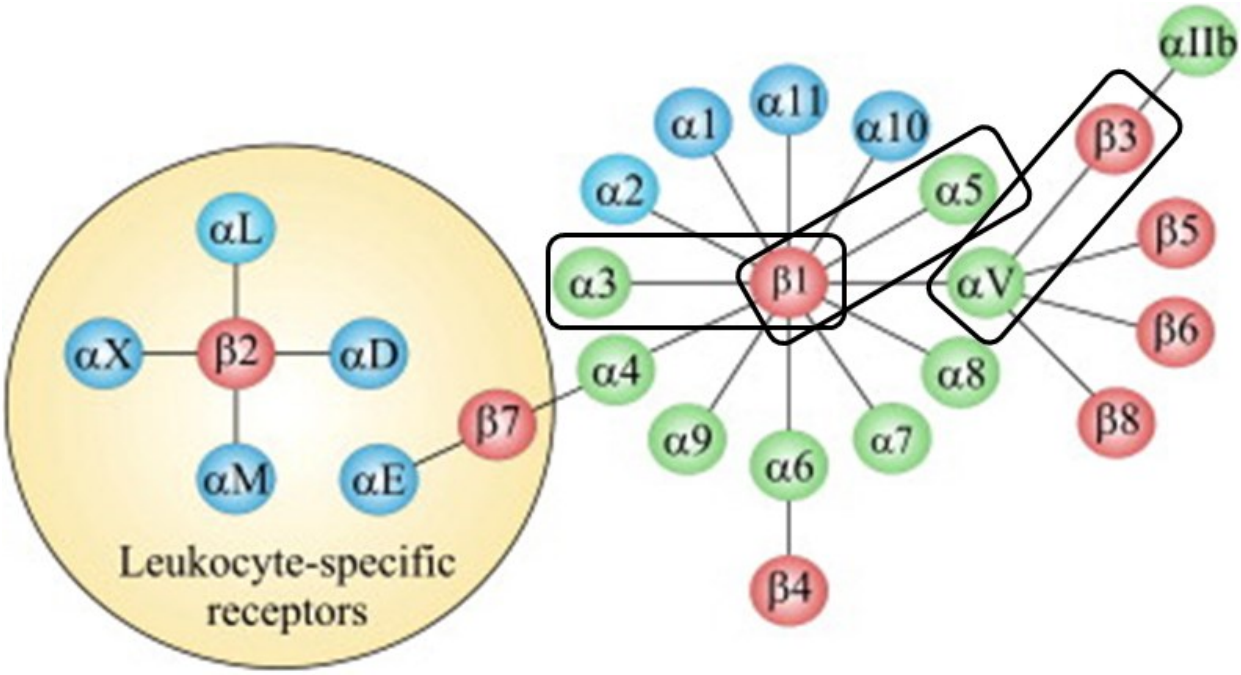

Figure 1.3 The integrin superfamily. There are 18 α-subunits and 8 β-subunits. Subunit partners are indicated by lines. The integrins expressed during *Xenopus laevis* gastrulation are in rectangle boxes (αVβ3, α3β1 and α5β1). (Adapted from Gahmberg et al., 2009)

1.4 IPP Complex

The IPP complex consists of ILK (integrin-linked kinase), PINCH (particularly interesting cysteine-histidine rich protein), and parvin (Figure 1.4). The ternary IPP complex is formed in the cytosol and recruited to integrin β1 and β3 cytoplasmic tails in response to integrin adhesion (Zhang et al., 2002). In both mammalian tissue culture cells and *Drosophila* wing epithelium, the stability of the IPP complex is interdependent on all three members (Zhang et al., 2002; Vakaloglou et al., 2012).

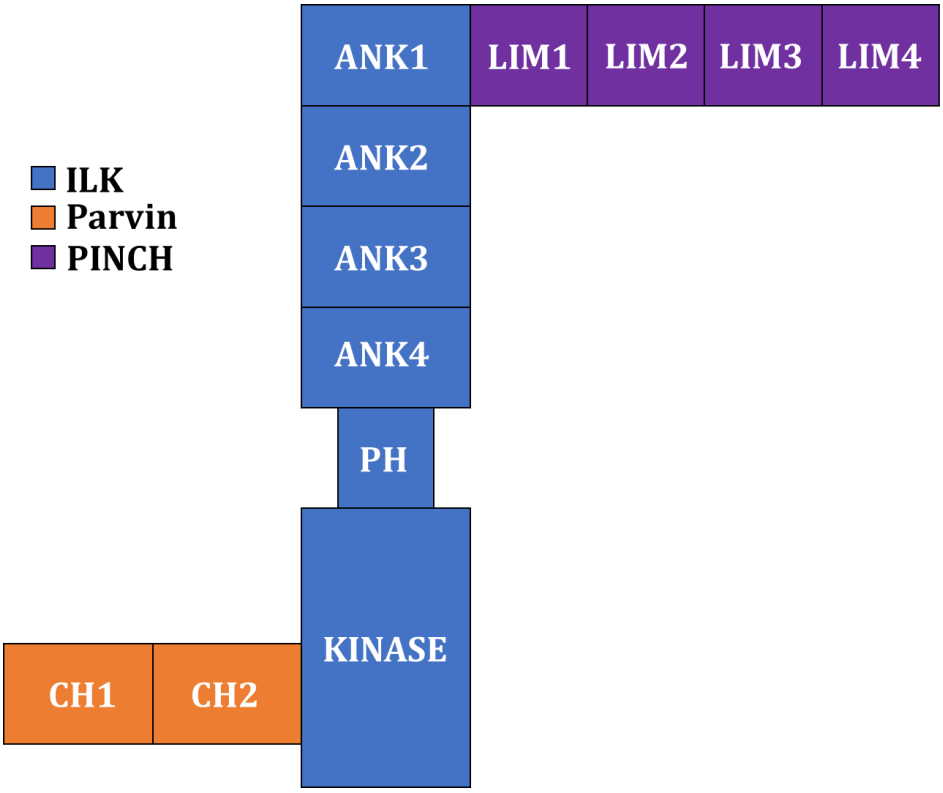

Figure 1.4 The ILK-PINCH-Parvin (IPP) complex and their domains. Integrin-linked Kinase (ILK) is the central scaffold of the complex, consisting of four repeating N-terminal ankyrin (ANK) domains. ILK also features a C-terminal kinase-like domain and an intermediate pleckstrin homology (PH) domain. Particularly Interesting New Cysteine Histidine-rich protein (PINCH) consists of four repeating LIM (Lin11, Isl-1, Mec-3) domains. Parvin has two calponin homology (CH) domains. (Adapted from Legate et al., 2006).

1.4.1 ILK

Integrin-linked kinase (ILK) is a highly conserved protein and first identified in a yeast two-hybrid screen using β1 integrin tail subunit as bait (Hannigan et al., 1996; reviewed in Legate et al., 2006). The N- terminal domain of ILK contains four ankyrin-like repeats (Figure 1.4) that meditate protein-protein interactions (Hannigan et al., 1996). The C-terminus shares sequence homology to Serine/Threonine protein kinases although there are conflicting reports whether ILK has catalytic activity (reviewed in Legate et al., 2006). ILK is the central molecule of the IPP complex. The N-terminal ankyrin repeat recruits PINCH while the C-terminal kinase like domain binds parvins and β1 and β3 cytoplasmic integrin tails (reviewed in Dagnino, 2011; Legate et al., 2006; Hannigan et al., 1996). In addition to PINCH and parvin, ILK has additional binding partners, suggesting a role as a central scaffolding molecule for protein complex assembly (reviewed in Zervas & Brown, 2002). Expression of soluble ankyrin domains fail to rescue ankyrin domain deletions in ILK suggesting both domains are required on the same molecule to act as a scaffold between proteins (Zervas et al., 2011).

Experiments in invertebrates such as *C. elegans* and *Drosophila melanogaster* indicate that ILK serves as a necessary leading component for IPP complex assembly recruiting both PINCH and parvin in muscle cells (Lin et al., 2003; Zervas et al., 2011). In *Drosophila melanogaster*, ILK is required to link integrin containing junctions of embryonic muscle attachment sites to the actin cytoskeleton (Zervas et al., 2011). ILK is also necessary and sufficient for subcellular localization of parvin to muscle attachment sites (Vakaloglou et al., 2012). However, parvin is not required for ILK recruitment in *C. elegans* (Lin et al.,

2003), nor is PINCH required in both *C. elegans* and *Drosophila* (Lin et al., 2003; Clark et al., 2003). These findings suggest the formation of the ternary IPP complex differs between vertebrates and invertebrates.

In *Xenopus* embryos, knockdown of ILK decreased adhesion of embryonic cells to FN substrate as well as inhibition of blastopore closure and convergent extension defects. ILK knockdown also decreased cell-cell adhesion and caused tissue to dissociate into single cells (Yasunaga et al., 2005). These embryo phenotypes match those observed when integrin-ECM binding is inhibited, suggesting ILK plays a role in integrin signaling and plays a role in regulating cell adhesion in *Xenopus* (Marsden & DeSimone, 2001; Marsden & DeSimone, 2003).

1.4.2 PINCH

PINCH is a member of the LIM (Lin-11, Isl-1, Mec-3) family of proteins and consists of five tandem LIM domains (Hannigan et al., 1996). The LIM1 domain of PINCH is responsible for interactions with ILK when forming the IPP complex (Hannigan et al., 1996). In mammals, there are two PINCH genes (reviewed in Legate et al., 2006). There is a single PINCH ortholog in invertebrates and *Xenopus* (Clark et al., 2003; Pilli, 2012).

In *Drosophila*, ILK recruitment to muscle attachment sites occurs independent of PINCH expression (Clark et al., 2003). Similar experiments in gastrulating *Xenopus* embryos also show independent behaviors between PINCH and ILK (Pilli, 2012). PINCH does not co-immunoprecipitate with ILK, and deletion of the LIM1 ILK binding domain does not inhibit PINCH localization to sites of integrin adhesion. Interestingly, it is suggested that PINCH is unlikely to be a member of the IPP complex *in vivo* (Pilli, 2012). Additionally, PINCH lies

downstream of growth factor receptors (reviewed in Legate et al., 2006). In *Xenopus*, platelet derived growth factor (PDGF) and transforming growth factor-β (TGF-β) signaling are essential for regulation of cell adhesion (Veevers-Lowe et al., 2011; Ghil & Chung, 1999). It is suggested Grb-4 links PINCH to these growth factor receptors through interactions with the PINCH LIM4 domain (Pilli, 2012). As such, the role of IPP *in vitro* may be to integrate growth factor signaling with cell adhesion.

1.5 Parvin

Parvins are a family of small scaffolding proteins recruited by ILK. Parvins consist of two functional calponin homology (CH) domains flanking an interim linker sequence. CH domains are a 100 amino acid domain found in a variety of proteins involved in signaling or cytoskeletal functions.

There are different families of CH domains characterized by their number and binding properties. Type 1 and type 2 CH domains often appear in tandem while type 3 CH domains appear alone in CH domain proteins. The function of CH domains includes actin-crosslinking to signaling pathways, regulatory functions, and actin binding (Gimona et al., 2002). Analysis of parvin CH domains indicate they belong to a new phylogenetic branch; type 4 and type 5 CH domain families (Olski et al., 2001; Gimona et al., 2002). The parvin CH domains are unconventional, functioning as scaffolds, and are separated by a much larger 60 amino acid linker sequence. The second CH domain contains a conserved paxillin binding site and is also responsible for interactions with ILK in murine tissue culture systems (Olski et al., 2001; Gimona et al., 2002).

In mammals, there are three parvin paralogs, α, β, and γ; each being encoded on distinct genes. α-parvin and β-parvin are ubiquitously expressed, whereas γ-parvin is expressed exclusively in hematopoietic tissue (Olski et al., 2001). As there is no hematopoietic tissue in early *Xenopus* embryos, I will not be discussing γ parvin further.

1.5.1 β-parvin

β-parvin was identified in a yeast two-hybrid assay using human ILK as bait (Yamaji et al., 2001). In Chinese hamster ovary (CHO) cells, β-parvin co-localizes with ILK to sites of focal adhesions (Yamaji et al., 2001). The CH1 domain is not required for ILK binding, while the CH2 domain mediates the interaction of β-parvin with ILK (Yamaji et al., 2001). β-parvin is also found in nascent cell surface membrane blebs of recently attached CHO cells (Yamaji et al., 2001). Over-expression of β-parvin CH2 domains resulted in deleterious effects on cell spreading. This suggests β-parvin regulates cell spreading through the CH2 domain. In well spread cells, β-parvin and ILK are found in the leading edge of lamellipodia at sites where focal adhesions are forming. This suggests β-parvin is involved with integrin-ILK signaling required for nascent focal adhesion structures (Yamaji et al., 2001).

1.5.2 α-parvin

Despite similar sequence identity to β-parvin, α-parvin has unique interactions. α-parvin was also identified in a yeast two-hybrid assay using human ILK as bait (Tu et al., 2001). In CHO and mouse fibroblast cells, α-parvin localizes to sites of focal adhesion and associates with the actin cytoskeleton (Tu et al., 2001; Olski et al., 2001). The CH1 domain of α-parvin shares similarity with the CH1 domain of β-spectrin. The CH1 domain of β-spectrin connects F-actin to other filament networks, but this interaction remains

unexplored in α-parvin CH1 (Gimona et al., 2002). In *C. elegans*, the CH1 domain is also necessary for downstream events leading to myofibrillogenesis. Conversely, this domain is not necessary for proper localization of α-parvin to focal adhesion sites (reviewed in Sepulveda & Wu, 2006). On the other hand, the CH2 domain is necessary and sufficient for α-parvin-ILK binding and localization to focal adhesions in CHO cells (Tu et al., 2001). This localization is dependent on interaction with ILK, as point mutations in the CH2 ILK binding domain impaired localization to focal adhesions (Tu et al., 2001). Cell adhesion assays performed with CHO and mouse myoblast tissue culture cells determined α-parvin is involved with the regulation of cell adhesion to collagen, and over-expression of the α-parvin CH2 domain significantly hindered cell adhesion (Tu et al., 2001). This suggests that cell adhesion is regulated through a necessary interaction between the CH2 domain of α-parvin and ILK. In addition to ILK, the CH2 domain also has been described to interact with paxillin (Nikolopoulos & Turner, 2000) although no functional role has been described.

1.5.3 Antagonistic relationship between α-parvin and β-parvin

Although found in the same cells, α-parvin and β-parvin appear to serve antagonistic functions and possibly act to regulate the expression of each other. In Hela cells, depletion of α-parvin expression resulted in increased levels of β-parvin, and likewise, over-expression of α-parvin results in reduced levels of β-parvin. This suggests α-parvin negatively regulates the cellular levels of β-parvin (Zhang et al., 2004). Furthermore, α-parvin and β-parvin appear to have an antagonistic interaction with ILK. In an immunoprecipitation experiment done in Hela cells overexpressing β-parvin or the CH2 domain, there was an increase in binding to ILK while α-parvin binding to ILK was reduced.

This suggests that β-parvin and α-parvin bind competitively to ILK and are mutually exclusive (Zhang et al., 2004).

1.6 β-parvin in *Xenopus*

β-parvin mRNA is expressed throughout embryogenesis and localized to the blastocoel roof and DMZ during gastrulation (Studholme, 2013). In a study of β-parvin function, deletion constructs were created to isolate the CH1 domain (RP1) and CH2 (RP2) domains. Over-expression of the CH1 domain resulted in inhibition of blastopore closure in stage 12 embryos. It also inhibited epiboly and mesoderm attachment to the blastocoel roof during gastrulation (Studholme, 2013). This is likely due to the CH1 domain inhibiting FN matrix assembly. FN matrix assembly is dependent on α5β1integrin (Marsden & DeSimone, 2003), but the CH1 domain of β-parvin does not interact with ILK, suggesting an alternative mechanism for FN matrix assembly inhibition. A crucial step in FN matrix assembly is tension across the blastocoel roof, which is a result of increased cell-cell adhesion through C-cadherin and actin cytoskeleton assembly (Dzamba et al., 2009). The CH1 domain was found at sites of nascent cell-cell adhesion *in vivo* and *ex vivo* and over-expression resulted in a decrease of C-cadherin adhesion by approximately 21% (Studholme, 2013). A 20 % decrease of C-cadherin adhesion was enough to inhibit FN matrix assembly (Dzamba et al., 2009) which suggests the mechanism by which the CH1 domain inhibits FN matrix assembly is by decreasing C-cadherin cell adhesion (Studholme, 2013). The CH1 domain was determined to be capable of influencing cell-cell adhesion through modulation of small GTPase signaling (Studholme, 2013). When the CH1 domain is overexpressed in embryos, FN assembly is inhibited without changing cell adhesion to FN. This has been attributed to

the downstream activation of Rac1 by the CH1 domain. It is unclear how this is occurring, but cell adhesion and behaviours requires a balance in small GTPase activation (Park et al., 2011).

The RP2 deletion construct isolates the CH2 domain of β-parvin. In the IPP complex, the β-parvin CH2 domain mediates interactions with ILK (Yamaji et al., 2001; reviewed in Legate et al., 2006). Co-immunoprecipitation experiments showed that both full-length β-parvin and RP2 are recruited by ILK in *Xenopus* (Studholme, 2013; Knapp, 2018). This recruitment is dependent on interactions between ILK and α5β1integrin, as deletions to the domain of ILK that interact with integrin fail to recruit β-parvin (Knapp, 2018). The CH2 domain localizes to focal adhesions in *Xenopus* A6 tissue culture cells and the basal surface of post-involution mesoderm cells (Studholme, 2013). Over-expression of the CH2 domain showed similar phenotypes to over-expression of the CH1 domain, such as failure of mesoderm attachment to the blastocoel roof and lack of FN matrix assembly. However, the β-parvin CH2 domain does not decrease cadherin adhesion like the CH1 domain, suggesting direct interference of integrin adhesion (Studholme, 2013). This is confirmed in cell adhesions assays where over expression of the CH2 domain inhibits both adhesion and cell migration on FN (Studholme, 2013; Knapp, 2018).

Full length β-parvin over-expression resulted in little to no effect on embryo morphogenesis, whereas co-expression of the individual CH1 and CH2 domains resulted in phenotypes more destructive than individual constructs; suggesting linkage of the two domains is necessary for normal signaling in the embryo (Studholme, 2013). The above

evidence suggests that decoupling the two CH domains found in parvin provides insights into how this molecule and the IPP complex can influence integrin function.

1.7 Summary

Xenopus laevis embryonic development is a well characterized process that is dependent on regulation of integrin and cadherin adhesion. The cell movements are well understood and provide a simple model to study the mechanisms and signaling pathways associated with integrin and cadherin adhesion. Since the tissue rearrangements of gastrulation are dependent on α5β1integrin mediated cell adhesion (Marsden & DeSimone, 2003), I hypothesize that *Xenopus* α-parvin regulates integrin mediated adhesion as a downstream participant of α5β1signaling during gastrulation. I aim to isolate *Xenopus laevis* α-parvin and perform a phylogenetic analysis on the amino acid sequence. Next, I will generate a temporal expression profile for α-parvin throughout *Xenopus* embryogenesis. To elucidate a mechanistic role for α-parvin, I will create deletion constructs isolating the individual CH domains and use them to determine *in vitro* compartmentalization and *in vivo* phenotypic changes.

2.0 Materials and Methods

2.1 Cloning α-parvin

2.1.1 Isolation of a cDNA representing *Xenopus* α-parvin

A putative α-parvin sequence was identified using genomic data available on *Xenbase* (Genbank accession# XP_018112776). Primers were designed against the 5' and 3' ends of the coding sequence (Table 2.1).

Total RNA was extracted following the standard protocol of easy-BLUE™ Total RNA Extraction Kit (iNtRON Biotechnology DR). Briefly, 20 embryos were lysed in 1 mL of easy-BLUE™ solution and then vortexed until no visible clumps of tissue remained ensuring complete cell lysis. 200 µl of chloroform was added to the lysate and briefly vortexed. The aqueous fraction was isolated by centrifugation at 13,000 G, 4°C for 10 minutes. 400 µl of the upper aqueous layer was transferred to a separate 1.5 mL tube with 400 µl of isopropanol to precipitate the RNA. The mixture was incubated at room temperature (RT) for 10 minutes and centrifuged at 13,000 G, 4°C for 5 minutes to obtain an RNA pellet. The pellet was washed using 1mL of 70% ethanol and centrifuged for an additional 5 minutes at 13,000 G, 4°C. The supernatant was removed, and the pellet dried at RT. The RNA pellet was resuspended in 100 µl of water, 10 µl of 5M ammonium acetate was added and mixed thoroughly, then 250 µl of chilled 100% ethanol was added, and the solution was left at -20°C overnight. RNA was collected by centrifugation at 13,000 G, 4°C for 10 minutes. The RNA pellet was washed with 70% ethanol and centrifuged at 13,000 G, 4°C for 5 minutes. The RNA pellet was dried and resuspended in 25 µl of water and kept on ice.

Table 2.1 PCR primers used to isolate α-parvin, RP1, and RP2 sequences. Underlined sequences correspond to restriction enzyme site added to primers to facilitate cloning.

Primer Sequence	Restriction Enzyme Sites
α-parvin (ATG) FWD	*BamHI*
5' – CCGGATCCATGGCAACGTCCCCCCAAAAATCTCC – 3'	
α-parvin REV	*XhoI*
5' - GGCTCGAGCTCCACGCTTCTGTACTTGGTG – 3'	
α-parvin FWD	*BamHI*
5' – CCGGATCCGCAACGTCCCCCCAAAAATCTCC – 3'	
α-parvin REV	*XhoI*
5' - GGCTCGAGCTCCACGCTTCTGTACTTGGTG – 3'	
α-parvin (ATG) FWD	*BamHI*
5' – CCGGATCCATGGCAACGTCCCCCCAAAAATCTCC – 3'	
RP1 REV	*XhoI*
5' – GGCTCGAGTCAAACGACGACTTGAATTGATACATGATCTGG – 3'	
α-parvin FWD	*BamHI*
5' – CCGGATCCGCAACGTCCCCCCAAAAATCTCC – 3'	
RP1 REV	*XhoI*
5' – GGCTCGAGTCAAACGACGACTTGAATTGATACATGATCTGG – 3'	
RP2 FWD	*BamHI*
5' – CCCGGATCCCAGAAGCTGGACGGAATGTTGC – 3'	
α-parvin REV	*XhoI*
5' - GGCTCGAGCTCCACGCTTCTGTACTTGGTG – 3'	

The concentration of total RNA was determined using an Ultraspec 2100 Pro spectrophotometer (GE Healthcare, Mississauga, ON). Total RNA was visualized on a 1% agarose gel to confirm integrity. First strand cDNA was synthesized using protocol from RevertAid™ H Minus First Strand cDNA synthesis kit (Fermentas, Burlington, ON). cDNA synthesis was initiated by combining a primary mixture of 2 μg of total RNA, 0.2 μg of

random hexamer primers and water up to 12 µl at 4°C. The mixture was incubated for 5 minutes at 70°C and then chilled on ice. The mixture was brought up to a final volume of 20 µl by adding 4 µl 5X ProtoScript® II Reverse Transcriptase Reaction Buffer (New England Biolabs (NEB), Toronto, ON), 40 units of Murine RNase inhibitor (NEB, Toronto, ON), 2 µl 10 mM dNTP mix (Thermo-Fisher, #R0192) and 200 units of ProtoScript® II Reverse Transcriptase (NEB, Toronto, ON). The mixture was incubated for 20 mins at 25°C and then for 2 hours at 42°C. The reaction was stopped by heating at 70°C for 10 minutes and chilling on ice.

2.1.2 Isolation of cDNA representing α-parvin

Full length α-parvin was isolated by PCR in a 50 µl reaction using 0.5 µl 10 mM α-parvin (ATG) FWD primers (Table 2.1), 0.5 µl 10 mM α-parvin REV primers (Table 2.1), 1 µl 10 mM dNTPs, 5 µl of 10X PCR buffer (NEB, Toronto, ON), 2 µl of first strand cDNA (section 2.1.1) as a template and 1.25 units of *Taq* polymerase (NEB, Toronto, ON). Cycling conditions were 2 minutes at 95°C, followed by 30 amplification cycles consisting of: 30 seconds at 95°C, 30 seconds at 58°C, and 90 seconds at 68°C. An additional 5 minutes at 68°C was included at the end of the last cycle.

TA cloning vector was created using a modified version of the protocol found in Marchuk et al., 1991. 1 µg of Bluescript II SK (-) vector was digested in a 50 µl reaction using 10 units of *Eco*RV restriction enzyme (NEB, Toronto, ON) for 1 hour at 37°C. *Eco*RV was denatured by heating at 75°C for 20 minutes. Overhanging T was generated in a 50 µl mixture of 1X Taq buffer, 2 µl 100 mM dTTP (NEB, Toronto, ON), and 1.25 units of *Taq* polymerase, incubated at 72°C for 1 hour. The vector was purified using on a column using

EZ-10 Spin Column DNA Gel Extraction Kit (Bio Basic, Markham, ON). The putative α-parvin insert was ligated with a 3:1 insert to vector molar ratio in a 20 µl reaction using 1X T4 ligase buffer (NEB, Toronto, ON) and 800 units of T4 DNA ligase (NEB, Toronto, ON). Ligations were incubated at RT for 3 hours. 10 µl of ligation was used to transfect 100 µl competent XL-1 Blue *Escherichia coli* (Stratagene, La Jolla, CA).

300 µl of Luria-Bertani medium (LB; 1% tryptone (w/v), 0.5% yeast extract (w/v), 1% NaCl (w/v)) was added to the cells and incubated at 37°C for 30 minutes. 200 µl and 50 µl of the cells were streaked onto LB-agar plates (LB with 1.5% agar (w/v)) containing 50 µg/mL ampicillin. The plates were incubated overnight at 37°C. Colonies were selected from the plate and inoculated in 2.5 mL LB containing 50 µg/mL ampicillin and incubated with agitation overnight at 37°C. Plasmids were recovered using Bio Basic EZ-10 Spin Column Plasmid DNA Miniprep Kit (Bio Basic, Markham, ON). Presence of insert was confirmed by digestion with *Bam*HI (NEB, Toronto, ON) and *Xho*I (NEB, Toronto, ON). The PCR insert was sequenced (Robarts Institute, Western University) and confirmed to be α-parvin by comparison to the potential α-parvin sequence retrieved from GenBank (Accession# XP_018112776).

2.1.3 Sub-cloning α-parvin

The α-parvin cDNA was removed from the TA vector using *Bam*HI and *Xho*I and ligated into the *Bam*HI and *Xho*I sites of Bluescript II (SK-) to generate the FLAP-BS construct. Ligations were performed as described in section 2.1.2. FLAP-BS was transfected and cloned as described in section 2.1.2. This construct was used for all subsequent sub-cloning procedures.

2.1.4 α-parvin Deletion Constructs

The RP1 deletion construct containing the CH1 domain of α-parvin (amino acids 1-217 of *Xenopus* α-parvin) was isolated using PCR (see below) (Figure 2.2). The primers used for PCR are described in Table 2.1 (**α-parvin (ATG) FWD and RP1 REV**). The RP2 deletion construct containing the CH2 domain of α-parvin (amino acids 218-397 of *Xenopus* α-parvin) was isolated using PCR (see below) (Figure 2.2). The primers used for the PCR are described in Table 2.1 (**RP2 FWD and α-parvin REV**).

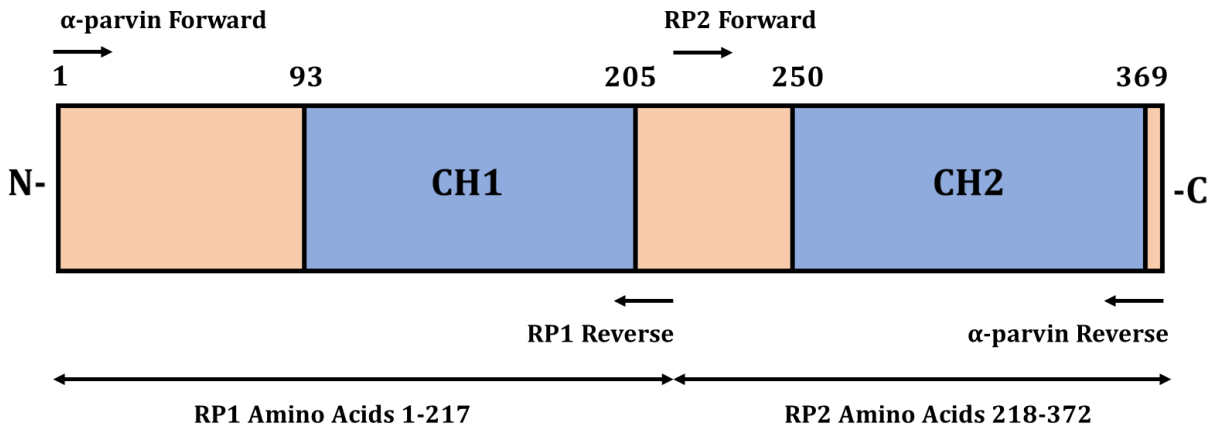

Figure 2.2 α-parvin RP1 and RP2 deletion constructs blueprint. α-parvin has two calponin-homology (CH) domains. Deletion constructs that isolate CH1 (RP1) and CH2 (RP2) were made according to this blueprint. Single headed arrows indicate forward and reverse primers. Double headed arrows indicate RP1 and RP2 deletion constructs.

The RP1 and RP2 deletion constructs were created using PCR in a 50 µl reaction using 0.5 µl 10 mM FWD primers (Table 2.1), 0.5 µl 10 mM REV primers (Table 2.1), 1µl 10 mM dNTPs, 5 µl of 10X PCR buffer (NEB, Toronto, ON), 0.1 ng of FLAP-BS as a template and 1.25 units of *Phusion* HF (NEB, Toronto, ON). PCR was performed as described in section 2.1.2.

The RP1 and RP2 inserts were digested using *Bam*HI and *Xho*I and ligated into the *Bam*HI and *Xho*I sites of Bluescript SK II (-) to generate the RP1-BS and RP2-BS constructs. Ligations were performed as described in section 2.1.2. RP1-BS and RP2-BS were individually transfected and cloned as described in section 2.1.2.

2.1.5 GFP Fusion Constructs

For *in vivo* imaging I created GFP tagged versions of the α-parvin, RP1, and RP2 constructs. RP2 inserts were isolated using PCR as described in section 2.1.4. FLAP and RP1 inserts omitting the ATG start site were generated using PCR. The primers used for PCR are described in Table 2.1 (**α-parvin FWD and α-parvin REV, α-parvin FWD and RP1 REV**). PCR was performed as described in section 2.1.2. FLAP, RP1, or RP2 inserts were digested using *Bam*HI and *Xho*I and ligated in frame into the *Bam*HI and *Xho*I sites of pCS2 GFP-N1 vector (gift from Jeff Miller). Ligations were performed as described in section 2.1.2. GFP-FLAP, GFP-RP1 and GFP-RP2 were individually transfected and cloned as described in section 2.1.2. The open reading frames were confirmed by sequencing (Robarts Institute, Western University).

2.2 *in vitro* mRNA Transcription

Fusion constructs were linearized using *Not*I HF (NEB, Toronto, ON) restriction enzyme. Linear plasmids were purified using EZ-10 Spin Column DNA Gel Extraction Kit (Bio Basic, Markham, ON). *In vitro* transcription reactions were carried out in 50 µl volumes containing 1 ug of linearized plasmid, 1X SP6 RNA polymerase reaction buffer (NEB, Toronto, Ontario), 1 mM rATP, 1 mM rCTP, 1 mM rUTP, 0.1 mM rGTP (Fermentas, Burlington, Ontario), 1 mM m7G(5')ppp(5')G RNA Cap Structure Analog (NEB, Toronto, Ontario), and 40 units of Riboblock RNase Inhibitor (Fermentas, Burlington, Ontario). 100 units of SP6 RNA polymerase (NEB, Toronto, Ontario) was added and the reaction was incubated at 37°C in a water bath for 30 minutes. 1.25 µl of 0.5 mM rGTP was added and the reaction was incubated at 37°C for 1 hour. The plasmid DNA was degraded with the addition of 3 units of RNase free DNase1 (NEB, Toronto, ON) and incubated at 37°C for 30 minutes. The mRNA was purified using Ambion Mega Clear Kit (Invitrogen, Burlington, Ontario) according to manufacturer instructions. The purified mRNA was precipitated by mixing 10 µl of 5M ammonium acetate thoroughly, adding 250 µl of chilled 100% ethanol and incubated at -20°C overnight. mRNA was collected by centrifugation at 13,000 G, 4°C for 10 minutes. The mRNA pellet was washed with 70% ethanol and centrifuged at 13,000 G, 4°C for 5 minutes. The mRNA pellet was dried and resuspended in 25 µl of water. mRNA quality was assessed using agarose gel electrophoresis and yields were determined using Ultraspec 2100 pro (GE Healthcare, Mississauga, ON). The mRNA stocks were aliquoted and stored at -80°C.

2.3 Tissue Culture

2.3.1 Maintenance of *Xenopus* A6 Cells

Xenopus laevis A6 kidney cells (ATCC# CCL-102, Rockville, MD) were cultured at RT in T70 flasks in 66% Leibovitz (L)-15 media, supplemented with 10% fetal bovine serum (v/v; FBS; Wisent, St. Bruno, QC), 1mM sodium pyruvate, 100units/mL penicillin, and 100ug/mL streptomycin (Wisent, St. Bruno, QC).

2.3.2 Transfection of *Xenopus* A6 Cells

Coverslips were cleaned in 66% nitric acid and 33% concentrated HCl. Clean coverslips were rinsed in water using a sonicator 3 times for 10 minutes and then air dried.

Cells were cultured until 70-80% confluence before being detached using Trypsin/EDTA (Wisent, St. Bruno, Quebec; 0.05% Trypsin, 0.53 mM EDTA), and replated on 250mm^2 bottom coated flasks in 66% L-15 media. Transfections were performed with Lipofectamine 3000 following manufacturer instructions. Cells to be transfected were rinsed with 66% L-15 media containing 2% FBS (v/v). Cells were incubated at RT for 4-5 hours in the presence of lipofectamine. The transfection media was removed, and the cells were incubated overnight in 2-3 mL of 66% L-15 media containing 2% FBS(v/v). Transfected cells were then moved onto coverslips (see above) in 30 mm^2 tissue culture dishes and left overnight in 2 mL of 66% L-15 media containing 2% FBS(v/v).

Cells were fixed in 4% paraformaldehyde in PBS (130 mM NaCl, 3 mM KCl, 10 mM Na_2HPO_4, 2 mM KH_2PO_4) for 15 minutes at RT. Cells were rinsed three times with PBS and permeabilized with 1% Triton X-100/PBS for 5 minutes. The cells were rinsed in PBS then

blocked with 1% bovine serum albumin (BSA; Sigma, Oakville, ON), 0.1% Triton X-100/PBS (BSA blocking solution) (Sigma, Oakville, ON) for 20 minutes. The cells were washed with BSA blocking solution three times for 10 minutes. Actin was stained with Rhodamine Phalloidin (Molecular Probes, Eugene, OR) in BSA blocking solution for 20 minutes at RT in the dark. The cells were then washed three times with BSA blocking solution for 10 minutes. Transfected cells were mounted on standard microscope slides using VECTASHIELD® mounting media with DAPI (Vector Laboratories, Inc., Burlingame, CA) and imaged using a Zeiss Axiovert 200 microscope (Zeiss, Mississauga, ON), Qimaging 1494 digital camera (Qimaging, Surrey, BC) and Open Lab Software (Improvision, Waltham, MA).

2.4 Maintenance and Manipulations of *Xenopus laevis* Embryos

Sexually mature *Xenopus laevis* were housed in the Department of Biology Aquatic Facility at the University of Waterloo. Female frogs are primed 3-7 days in advance with 50 units of human chorionic gonadotropin (hCG; Chorulon; Intervet, Kirkland, QC) through subcutaneous injection. Spawning was induced with 400 units of hCG. Eggs were obtained through manual stripping and placed in a Petri dish. Testes were surgically isolated from a male frog and stored in L-15 complete media. A small piece of minced testes was resuspended in 1mL 1X MBS (Modified Barth's Saline; 1X MBS; 88 mM NaCl, 1 mM KCL, 0.7 mM MgSO4, 1 mM HEPES, 5 mM NaHCO, 0.1 mM CaCl2, pH 7.6) and used to fertilize eggs for 2 minutes at RT. The fertilized embryos were flooded with water and left for 20 minutes at RT. Fertilized embryos were dejellied using a 2% L-cysteine in 0.1X MBS (pH 8.3) with gentle agitation. The embryos were rinsed three times with deionized water, and two times

in 0.1X MBS. The embryos were then transferred to a 100mm Petri dish with 0.1X MBS and cultured until desired stage.

2.5 Embryo Microinjections

Injections of mRNA were done using a Narishige IM300 pressure injector (East Meadow, NY). Glass microinjection needles were created using a Narishige PC-10 puller (East Meadow, NY). Embryos were injected in 4% Ficoll in 0.5X MBS. *In vitro* transcribed mRNA was injected (4nl) into the future dorsal side of stage 2 embryos at equimolar concentrations. Injected embryos were transferred to 0.1x MBS and cultured to desired stage for imaging.

2.5.1 Imaging

Whole embryos were fixed at the desired stage in 2% trichloroacetic acid (TCA)/water for 1 hour at RT and then transferred to 0.1% Tween-20 in PBS to be imaged using a Zeiss Lumar V12 stereomicroscope (Zeiss, Mississauga, ON) with Zeiss Axiovision 4.7 software (Zeiss, Mississauga, ON). GFP fluorescence was visualized in live embryos on a Zeiss Lumar V12 stereomicroscope (Zeiss, Mississauga, ON) using Zeiss Zen software (Zeiss, Thorndale, ON). Fixed embryos were bisected along the sagittal and lateral planes for imaging using a scalpel blade.

2.6 Western blotting

Western blots were prepared using standard methods (Sambrook & Russell, 2001). 5 stage 11.5 embryos were lysed in embryo solubilization buffer (ESB; 25 mM Tris (pH 7.5), 50 mM NaCl, 1% TritonX-100 (v/v), 1 mM PMSF (phenylmethyl sulfonyl fluoride), 1X

protease inhibitor cocktail (Roche, Mississauga, Ontario). Embryo lysate was centrifuged at 13,000 G, 4°C, for 15 minutes. The clear middle fraction was removed and denatured using 5X SDS sample buffer (312.5 mM Tris (pH 6.8), 25% glycerol, 10% sodium dodecyl sulfate, 50 mM 2-mercaptoethanol, 0.05% bromophenol blue) and heated at 95°C for 5 minutes. The samples were separated using 12% sodium dodecyl-sulphate polyacrylamide gel electrophoresis (SDS-PAGE) in Bio-Rad Mini-PROTEAN® II Apparatus (Bio-Rad, Mississauga, ON) and transferred onto a nitrocellulose membrane (GE Healthcare, Mississauga, ON) following the protocol in the Bio-Rad manual. The membrane was incubated overnight in western blot blocking solution (5% skim milk powder (w/v) in TBST (2 mM Tris, (pH 7.5), 30 mM NaCl, 0.1% Tween20 (v/v)). The membrane was incubated with 1:1000 mouse anti-GFP primary antibodies (Roche #11814460001) at RT for 1 hour. The membrane was washed with blocking solution 3 times for 10 minutes, and then incubated with 1:10000 anti-mouse HRP-conjugated secondary antibody (Jackson Immune Research #115035146) for 1 hour at RT. The membrane was washed in blocking solution 3 times for 10 minutes followed by a wash in TBS 2 times for 5 minutes. Proteins were visualized using luminol (2.5 mM luminol (Sigma #A-8511), 0.4 mM p-coumaric acid (Sigma#C-9008), 100 mM Tris-HCL (pH 8.5) and 0.02% hydrogen peroxide (v/v) 100 mM Tris-HCL (pH 8.5)). Membranes were imaged using Bio-Rad ChemiDoc MP Imager (Bio-Rad, Mississauga, ON).

3.0 Results

3.1 Isolation of *Xenopus laevis* α-parvin

The sequence data for α-parvin on *Xenbase* (Karimi et al., 2018) is based upon genomic data and no complete cDNA has been described. Therefore, my first goal was to isolate a cDNA representing *Xenopus laevis* α-parvin. *Xenopus laevis* is tetraploid, with two complete genomes known as the 'S(hort)' and 'L(ong)' genomes. As such, I expect that there are two homologs of α-parvin. RNA-seq data indicates that the 'L' genome is responsible for the majority, if not all, of α-parvin expression (*Xenbase*: Karimi et al., 2018, Session et al., 2016). Therefore, primers were designed to flank the open reading frame of the 'L'-homolog of α-parvin, starting at the 5' ATG start codon and ending at the 3' TGA stop codon (Table 2.1, designed by Justin Knapp, 2018). RNA-seq data on *Xenbase* indicates that α-parvin expression peaks at embryonic stage 9 (*Xenbase*: Karimi et al., 2018, Session et al., 2016). Therefore, I used total RNA isolated from stage 9 embryos to make single stranded cDNA to be used in RT-PCR.

The PCR generated a single product of 1119 bp (Figure 3.1). The PCR product was cloned into a TA vector (Bluescript II SK (-), section 2.1.2) and then sub-cloned into Bluescript II SK (-) with *Bam*HI and *Xho*I using restriction enzyme sites located in the primers (Table 2.1). Subsequent sequencing confirmed that the isolated cDNA represented *Xenopus laevis* α-parvin (99.5% identity with Genbank accession# XP_018112776) (Figure 3.2).

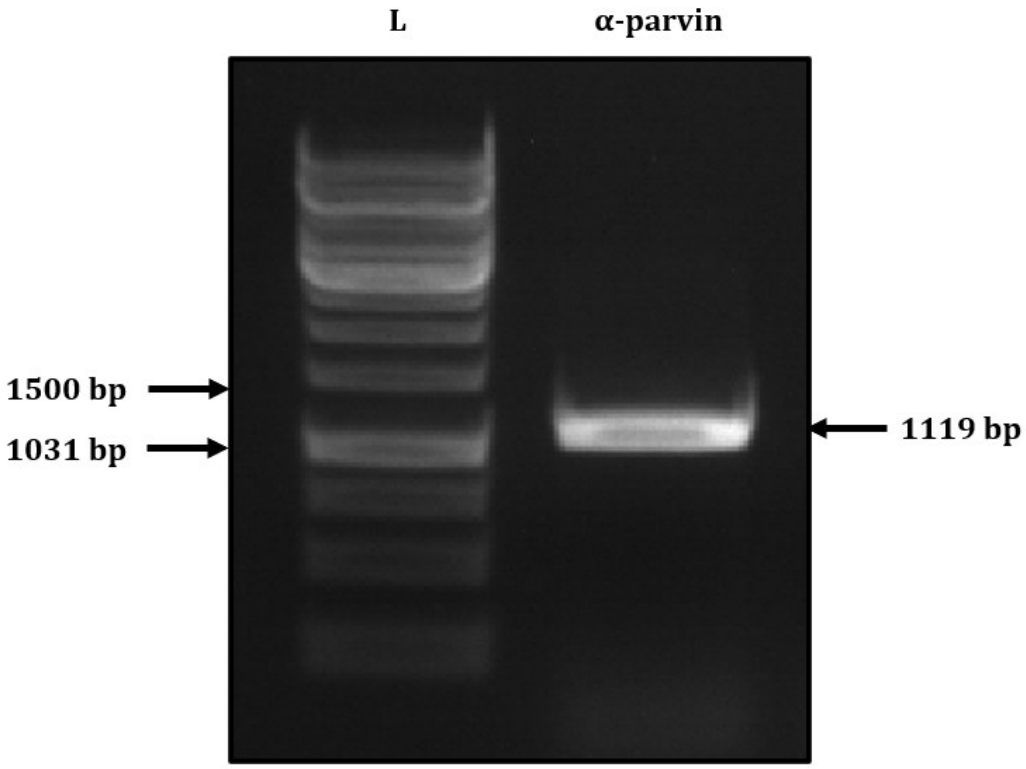

Figure 3.1 *Xenopus laevis* α-parvin RT-PCR. Total RNA was extracted from stage 9 embryos and used to synthesize single strand cDNA. RT-PCR revealed a single 1119 bp band that represents *Xenopus laevis* α-parvin.

3.2 Phylogenetic Analysis of *Xenopus* α-parvin

I compared the predicted amino acid sequence of the *Xenopus* α-parvin cDNA that I recovered to several α-parvin orthologs found in other model organisms (Figure 3.2). All the orthologs have the same number of amino acids (372), with the exception of *Drosophila melanogaster* (367 AA). The *Xenopus* α-parvin amino acid sequence shares high identity with other α-parvin orthologs: *Homo sapiens* (94%), *Mus musculus* (92%), *Gallus gallus* (93%), and *Danio rerio* (87%). The sequence shares the least identity with the single *Drosophila melanogaster* parvin (55%). The CH1 and CH2 domains in particular are highly conserved in vertebrates, with only 1 difference in amino acid sequence similarity in each domain.

The evolutionary divergence in amino acid sequence of α-parvin orthologs and β-parvin orthologs was visualized as a phylogram (Figure 3.3). The single *Drosophila melanogaster* parvin is the most divergent in sequence and represents a more ancestral parvin. Therefore, the *Drosophila melanogaster* parvin ortholog was selected as an outgroup to root the cladogram. The alignment of the amino acid sequences shows high conservation between α-parvin orthologs. As seen in Figure 3.3, *Xenopus* α-parvin clearly clusters with other α-parvin orthologs distinct from the β-parvin orthologs.

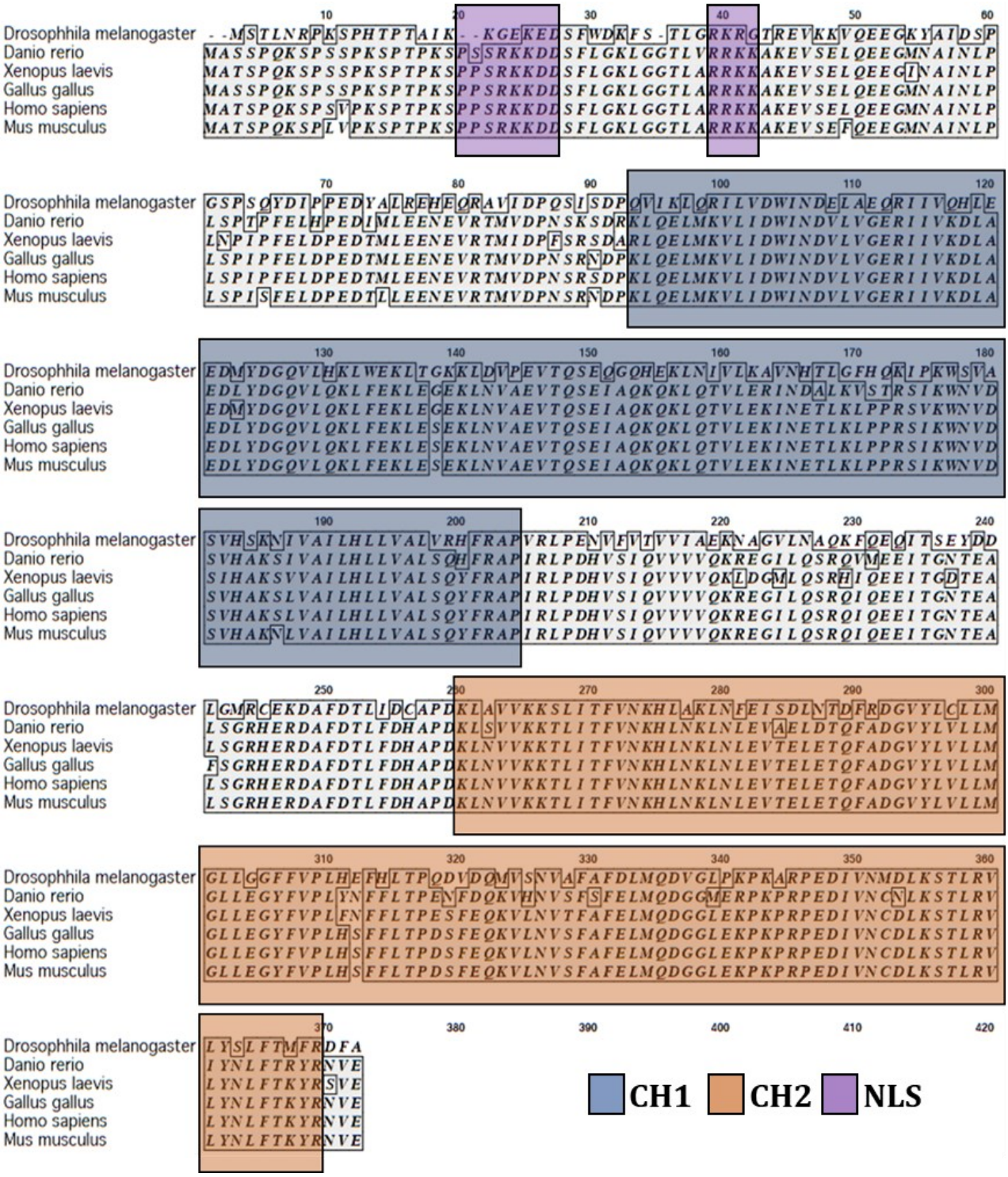
Drosophhila melanogaster
Danio rerio
Xenopus laevis
Gallus gallus
Homo sapiens
Mus musculus
CH1
CH2
NLS

Figure 3.2 *Xenopus laevis* α-parvin is highly conserved. The amino acid sequences of α-parvin orthologs from *Drosophila melanogaster* (NP_001285464.1), *Danio rerio* (NP_001002872.1), *Xenopus laevis* α-parvin cDNA sequence data, *Gallus gallus* (XP_040529478.1), *Homo sapiens* (NP_060692.3), and *Mus musculus* (EDL17031.1) were aligned with ClustalW. CH1 and CH2 domains are highlighted in blue and orange boxes. The nuclear localization sequences are marked in purple. Similarities are highlighted in grey. The formatted alignment was generated using MacVector software (MacVector Inc, Cary, NC)

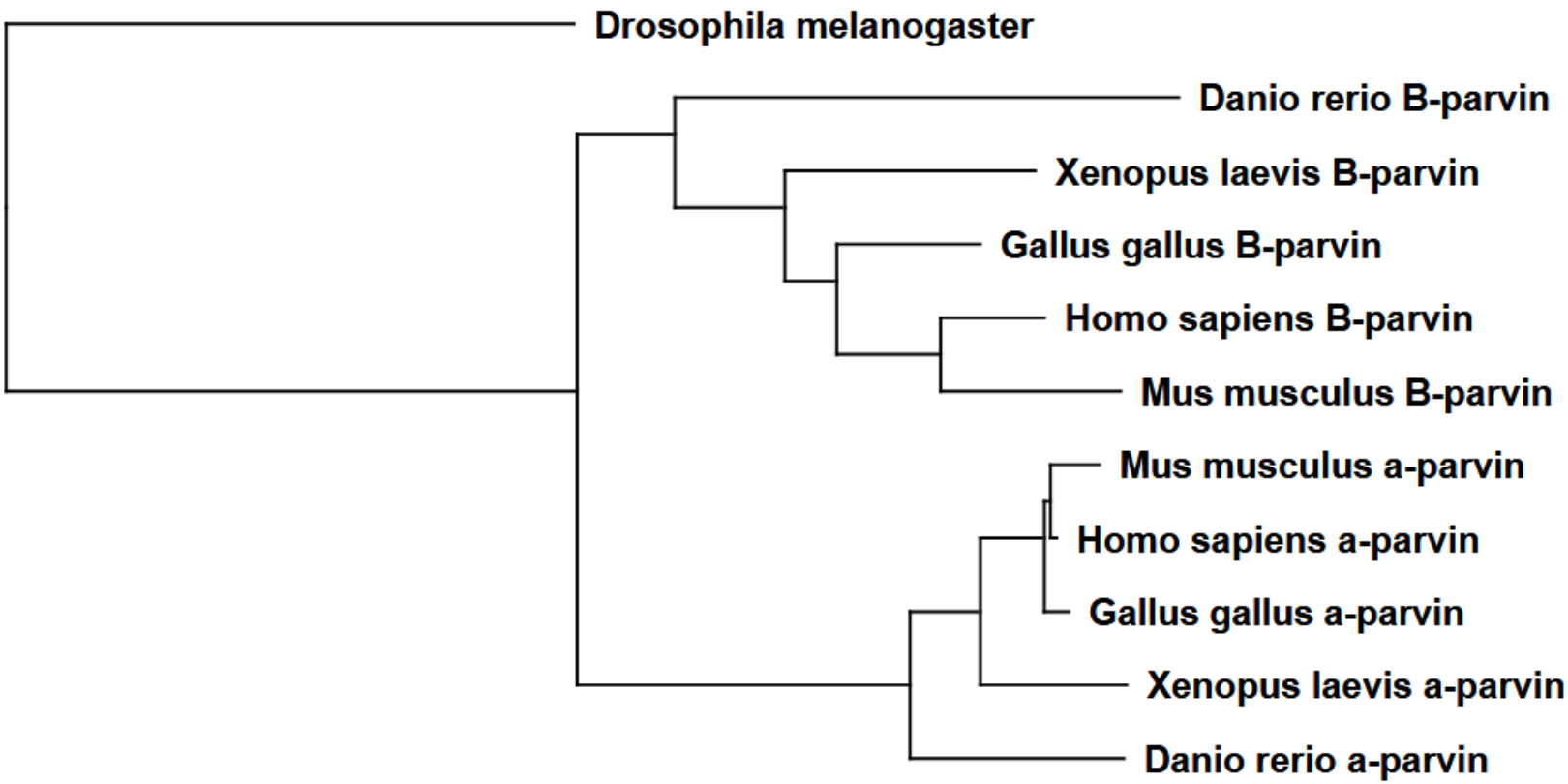

Figure 3.3 *Xenopus* α-parvin clusters with other α-parvins. A phylogram created using MacVector software (MacVector Inc, Cary, NC) depicting evolutionary divergence in amino acid sequence of α-parvin and β-parvin orthologs. Parvin ortholog sequences from *Drosophila melanogaster, Danio rerio, Xenopus laevis, Gallus gallus, Homo sapiens,* and *Mus musculus* were aligned with ClustalW. *Drosophila* parvin ortholog resembles an ancestral parvin and was selected as an outgroup due to high divergence from other sequences. β-parvin is more closely related to *Drosophila* parvin than α-parvin is, suggesting α-parvin is more recently evolved through a duplication event.

3.3 Temporal Expression of *Xenopus* α-parvin

I used RT-PCR (reverse transcriptase polymerase chain reaction) to analyze the temporal expression of *Xenopus laevis* α-parvin during early development. Total RNA was extracted from representative stages of embryonic development and used to generate single stranded cDNA to be used in RT-PCR. The PCR shows a single 1119 bp band at all stages (Figure 3.4). These results indicate that α-parvin is expressed as maternal mRNA prior to the onset of zygotic gene expression (Stage 2) and zygotically expressed after the mid-blastula transition (stage 7). There is continued expression of α-parvin through gastrulation (Stages 10, 11, 12), and into neurulation (Stage 17).

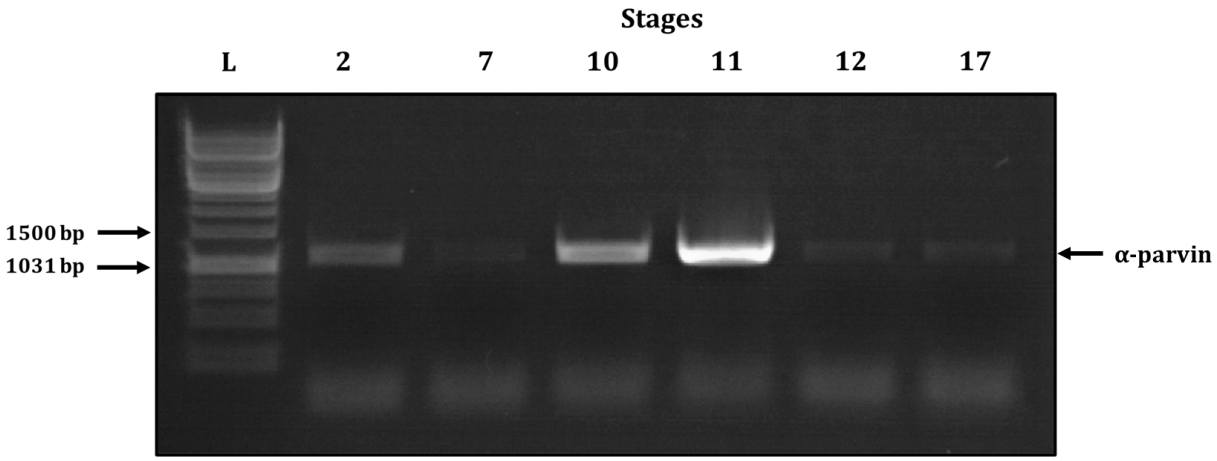

Figure 3.4 α-parvin mRNA is expressed throughout early *Xenopus* embryo development. RT-PCR was used to amplify endogenous α-parvin transcripts using total RNA isolated from *Xenopus* embryos of various developmental stages. α-parvin is expressed as maternal mRNA prior to the onset of zygotic gene expression (Stages 2) and zygotically expressed after the mid-blastula transition (stage 7), throughout gastrulation (Stages 10, 11, 12), and during neurulation (Stage 17).

3.4 α-parvin is recruited to sites of focal adhesion

3.4.1 Expression of Fusion Constructs

To examine the spatial recruitment of α-parvin I made GFP fusion constructs that isolate the CH1 (RP1) and CH2 (RP2) domains as well as full length α-parvin (FLAP, section 2.1.5). Constructs were cloned in frame to the carboxy terminus of eGFP in pCS2 GFP-N1 (section 2.1.5) to allow for *in vivo* visualization. My first step was to confirm the expression of GFP tagged constructs. I injected stage 2 embryos with mRNAs that represent GFP, GFP-FLAP, GFP-RP1 and GFP-RP2. These embryos were collected at stage 11 and used for western blots. Western blots using an antibody against GFP (Roche #1181446000) reveals that the constructs are being expressed as full-length proteins in embryos (Figure 3.5). As expected, in the lane representing uninjected embryos, there is no expression of GFP (Figure 3.5, Lane A). Full length α-parvin has an expected molecular weight of 42 kDa and the GFP-FLAP construct is expected to run at ~74 kDa (Figure 3.5, Lane B), the RP1 construct has a predicted molecular weight of 32 kDa and including the GFP tag runs at ~56 kDa (Figure 3.5, Lane C). The RP2 deletion construct with the GFP tag is expected to run at ~50 kDa (Figure 3.5, Lane D). eGFP has a molecular weight of 32 kDa (Figure 3.5, Lane E). Therefore, I see proteins in the expected range on the Western blot for each GFP tagged construct and confirm that they are being expressed as a fusion protein.

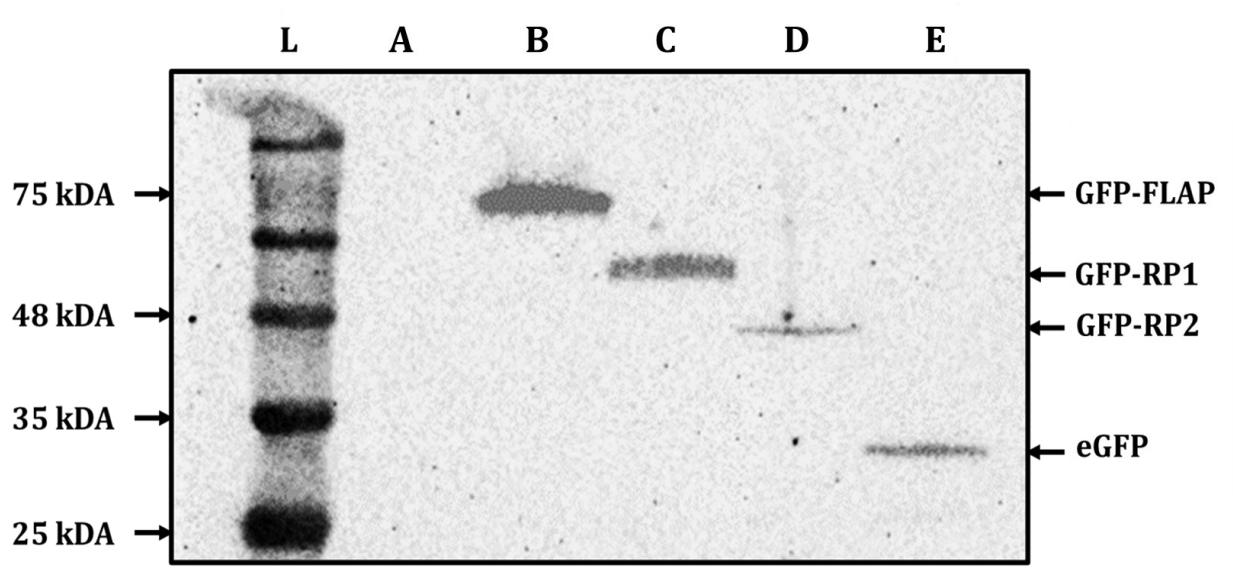

Figure 3.5 GFP-tagged constructs are expressed as fusion proteins in embryos. Stage 2 embryos were injected with GFP or α-parvin GFP fusion constructs in the future dorsal side and cultured until stage 11.5. Total proteins were extracted from embryos and separated using SDS-PAGE. GFP was revealed using mouse anti-GFP antibody (Roche #1181446000).

3.4.2 Localization of GFP-α-parvin in *Xenopus* A6 cells

Previous studies in mammalian cells show that both α-parvin and β-parvin localize to focal adhesions and that this is dependent on the CH2 domain interaction with ILK (Tu et al., 2001; Yamaji et al., 2001). In *Xenopus*, GFP tagged full length β-parvin and the RP2 construct co-localize with ILK to focal adhesions in *Xenopus* A6 tissue culture cells (Studholme, 2013). In order to visualize the compartmentalization of *Xenopus* α-parvin, I used a similar approach and transfected *Xenopus* A6 tissue culture cells with plasmids containing GFP-FLAP (Figure 3.6, A1-A3), GFP-RP1 (Figure 3.6, B1-B3), and GFP-RP2 (Figure 3.6, C1-C3). GFP-FLAP expression and compartmentalization is visualized in panel A1-A3 (Figure 3.6). In panel A1, GFP-FLAP expression (green), actin stained with Rhodamine Phalloidin (red), and nuclei stained with DAPI (blue) are visualized together (Figure 3.6). GFP-FLAP expression is shown in panel A2-A3 (Figure 3.6). The full length α-parvin construct is associated with sites of matrix adhesion, indicated by white arrows (Figure 3.6, Panel A3). GFP-RP2 expression and compartmentalization is shown in panel B1-B3 (Figure 3.6). As in panel A1, GFP-RP2 cells (green), actin (red), and nuclei (blue) are visualized together (Figure 3.6, B1). GFP-RP2 expression is visualized alone in panel B2-B3 (Figure 3.6). The construct isolating the second CH domain (GFP-RP2), known to interact with ILK, is also found in focal adhesions (Figure 3.6, Panel B3 arrows). The FLAP and RP2 constructs accumulate in the nucleus in addition to sites of cell adhesion (Figure 3.6, Panel A3, B3). Finally, GFP-RP1 expression and compartmentalization is visualized in panel C1-C3 (Figure 3.6). Like panel A1, GFP-RP1 expression is in green, actin in red, and nuclei in blue (Figure 3.6, C1). GFP-RP1 expression is isolated in panel C2-C3 (Figure 3.6). The construct isolating the first CH domain (GFP-RP1) is not found in focal adhesions (Figure 3.6, Panel

C3). The GFP-RP1 construct appears instead to associate with actin stress fibers and remains mostly cytosolic (Figure 3.6, Panel C3). Nuclear localization of the GFP-RP1 construct is not as strong as seen in GFP-FLAP and GFP-RP2 (compare Figure 3.6, panel A2, B2, C2).

3.4.3 Co-localization of GFP-α-parvin and RFP-β-parvin in *Xenopus* A6 cells

While both α-parvin and β-parvin localize to focal adhesions through interactions with ILK (Tu et al., 2001; Yamaji et al., 2001), they are mutually exclusive in their interaction with ILK in HeLa cells (Zhang et al., 2004). To ask if a similar relationship holds true in *Xenopus*, I co-transfected *Xenopus* GFP-α-parvin (GFP-FLAP) and RFP-β-parvin (RFP-FLBP) into A6 cells and asked if they co-localize to focal adhesions. In *Xenopus*, α-parvin and β-parvin are found together in focal adhesions (Figure 3.7, Panel A-C) as well as exclusive compartments (Figure 3.7, Panel B-C). In panel A (Figure 3.7), localization of GFP tagged α-parvin and RFP tagged β-parvin reveals co-localization of α-parvin and β-parvin to focal adhesions. The white box in A outlines the area magnified in panel B and C (Figure 3.7). The RFP-FLBP construct is found in focal adhesions in-between the arrows (Figure 3.7, Panel B). RFP-FLBP is more concentrated and appears to occupy less space in focal adhesions than GFP-FLAP (Figure 3.7 Panel B, C). GFP-FLAP is less concentrated than RFP-FLBP in those focal adhesions but appears to occupy exclusive space within the focal adhesions (Figure 3.7, Panel C). The GFP-FLAP construct is also found in unique focal adhesions (Figure 3.7, yellow arrows, Panel C). Therefore, α-parvin and β-parvin at least partially co-localize to focal adhesions in *Xenopus* A6 cells (Figure 3.7).

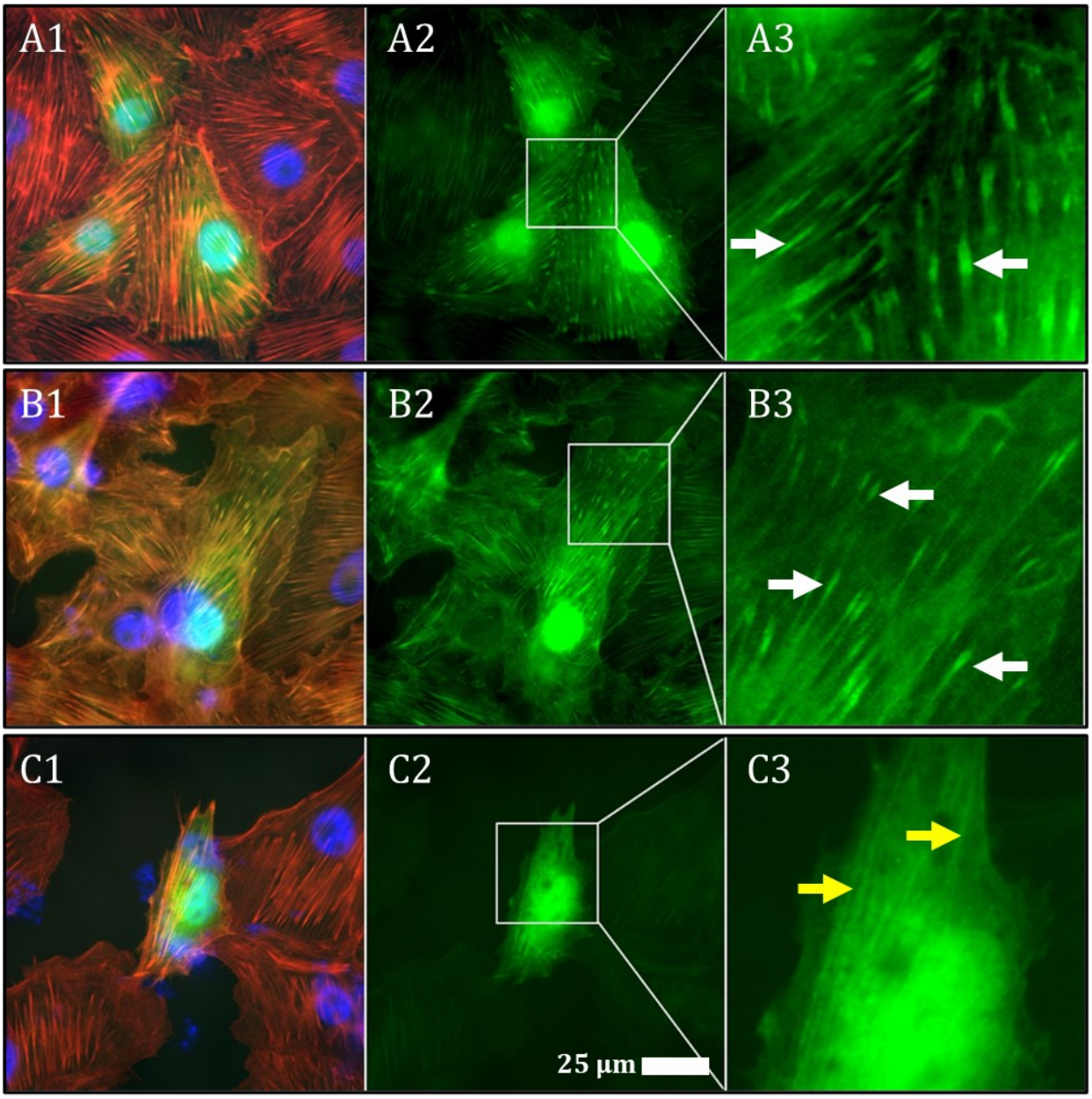
A1
A2
A3
B1
B2
B3
C1
C2
C3
25 µm

Figure 3.6 α-parvin and RP2 compartmentalize to focal adhesions in *Xenopus* tissue culture cells. *Xenopus A6* cells were transfected with GFP-FLAP, GFP-RP1, or GFP-RP2 plasmids. Both protein expression and compartmentalization are visualized. The area inside the white boxes is magnified on panels to the right. GFP-full length α-parvin (A1-A3) and GFP-RP2 (B1-B3) proteins compartmentalized to focal adhesions. GFP-RP1 (C1-C3) proteins remain cytosolic and associate with actin stress fibers. White arrows indicate focal adhesions. Yellow arrows indicate actin stress fibers.

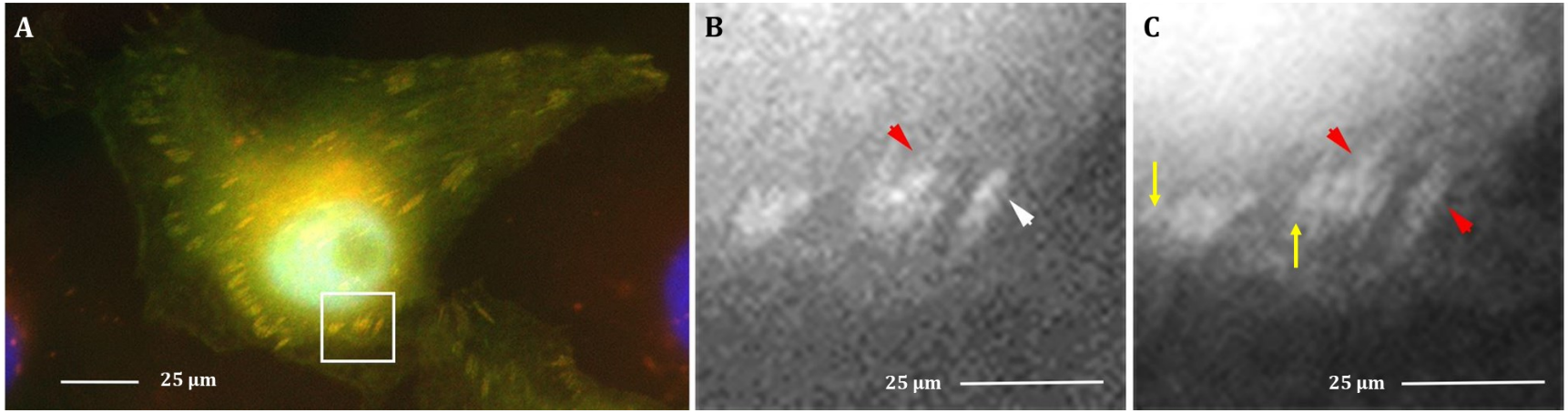

Figure 3.7 α-parvin and β-parvin partially co-localize to focal adhesions in *Xenopus* tissue culture cells. *Xenopus* A6 cells were co-transfected with GFP-FLAP, and RFP-FLBP (created by Catherine Studholme) plasmids. Both full length α-parvin and full length β-parvin proteins partially co-localize to focal adhesions (A). In-between the arrows are a series of focal adhesions. RFP-FLBP found in these focal adhesions cover a large area (B). The white arrow indicates a focal adhesion with stronger concentration of RFP-FLBP. GFP-FLAP is found exclusively in some focal adhesions (yellow arrow) (C).

3.5 A role for α-parvin in embryonic development

Since α-parvin constructs localize as expected in tissue culture cells (Figure 3.6), I then used these constructs to help describe a mechanistic role in *Xenopus* gastrulation. I performed over-expression experiments to examine roles for *Xenopus* α-parvin during early development. Previously, this approach was fruitful in describing a role for β-parvin (Yamaji et al., 2001, Studholme, 2013, Knapp, 2018).

I performed an initial experiment to titrate mRNA concentrations used in microinjections. I titred GFP-FLAP until it caused minimal disruptions to normal *Xenopus* development (data not shown). I then performed an injection trial with mRNA representing GFP, GFP-FLAP, GFP-RP1, and GFP-RP2 used at equimolar ratios. Embryos were injected at the two-cell stage in the future dorsal side. The embryos were cultured and then scored for embryo phenotypes (Figure 3.8). Embryos were scored as either normal, class 1 defects or class 2 defects (Figure 3.8). Class 1 defects include a hunched phenotype and retained blastocoel that produces belly blisters. Class 2 defects are more severe and include axial truncation and anterior defects . Control uninjected (n=32), GFP (n=19) and GFP-FLAP (n=38) injected embryos had very few defects (Figure 3.8). Control embryos exhibited 1 class 1 defect, hunched, and 1 class 2 defect, being severe axial truncation (Figure 3.8). GFP injected embryos only expressed 1 class 2 severe axial truncation defect (Figure 3.8). GFP-FLAP injected embryos displayed 4 class 1 defects, all retained blastocoel blisters. This group of embryos also exhibited 1 class 2 defect, a severe axial truncation (Figure 3.8). In comparison, GFP-RP1 (n=30) and GFP-RP2 (n=32) injected embryos had substantially more defects when compared to uninjected, GFP, and GFP-FLAP injected embryos (Figure

3.8). GFP-RP1 injected embryos displayed 9 class 1 defects such as retained blastocoel blisters or being hunched. This cohort of embryos also displayed 19 class 2 phenotypes, mostly severe axial truncations (Figure 3.8). GFP-RP2 injected embryos displayed 8 embryos with class 1 phenotypes, mostly represented by retained blastocoel blisters. A further 16 showed class 2 defects such as severe axial truncations and open blastopores (Figure 3.8). Therefore, RP1 and RP2 cause severe disruption to *Xenopus* embryos by the time they form hatching tadpoles.

Figure 3.8 Over-expression of RP1 and RP2 functional domains cause defects. Embryos were injected with mRNA transcripts representing GFP, GFP-FLAP, GFP-RP1, and GFP-RP2 at stage 2 in the future dorsal side and phenotypes were scored at stage 28. Class 1 defects (purple) include hunched phenotype and retained blastocoel blisters. Class 2 defects (orange) include axial truncation and missing heads. Embryos with no defects are shown in blue. Defects are found in 93.3% of RP1 injected embryos, and in 75% of RP2 injected embryos. Uninjected (6.3%), GFP (5.3%), and GFP-FLAP (13.2%) injected embryos display a minimal number of defects in the population.

3.5.1 CH1 and CH2 delay blastopore closure

Embryo phenotypes seen in the section above can be attributed to defects in the tissue movements that describe gastrulation. The dorsal lip forms at stage 10 on the exterior of the embryo as the DMZ involutes towards the interior of the embryo. The dorsal lip expands to become the ring-shaped blastopore that closes by late stage 12, signaling the end of gastrulation. Blastopore closure is driven by epiboly and convergent extension, both being integrin dependent processes. Since α-parvin plays a role in downstream signaling of integrin, I looked to see if over-expression of my constructs affected blastopore closure during gastrulation.

Embryos were injected in the future dorsal side with mRNA representing GFP, GFP-FLAP, GFP-RP1 and GFP-RP2 at the two-cell stage and cultured until stage 11.5. GFP expression was confirmed (Figure 3.9, A1-C1; Figure 3.10, A1-C1), and blastopore closure phenotypes were recorded in stage 11.5 embryos (Figure 3.9, A-C; Figure 3.10, A-C). GFP expression in the dorsal mesoderm around the blastopore confirms accurate tissue targeting of injections for all treatments (Figure 3.9, Panel B1-C1; Figure 3.10, Panel A1-C1). There is no GFP expression in the control uninjected embryos (Figure 3.9, Panel A1) and these embryos exhibit normal blastopore morphology characteristic of mid stage *Xenopus* gastrulation (Figure 3.9, Panel A). The blastopore size is decreasing as the embryo approaches the end of gastrulation at stage 12. The GFP tag alone causes no change in phenotype as compared to uninjected embryos (Figure 3.9, Panel B). Over-expression of GFP-FLAP also results in no visible differences in blastopore phenotypes compared to the controls (Figure 3.9, Panel C). As such, GFP and GFP-FLAP do not inhibit blastopore closure.

In contrast, embryos over-expressing GFP-RP1 and GFP-RP2 present different phenotypes compared to GFP expressing embryos (Figure 3.10, Panel A-C). Embryos over-expressing RP1 exhibit a wider blastopore diameter compared to the blastopores found in GFP expressing embryos (Figure 3.10, Panel A-B, black bars). The embryos over-expressing the CH2 domain (RP2) also exhibit wider blastopore diameters compared to GFP expressing embryos (Figure 3.10, Panel A, C). The GFP-RP2 expressing embryos show delayed blastopore closure when compared to GFP-RP1 expressing embryos (compare Figure 3.10, Panel B and C). Therefore, while over-expression of RP1 and RP2 constructs in embryos cause delays in blastopore closure, they are likely due to different mechanisms during *Xenopus* gastrulation.

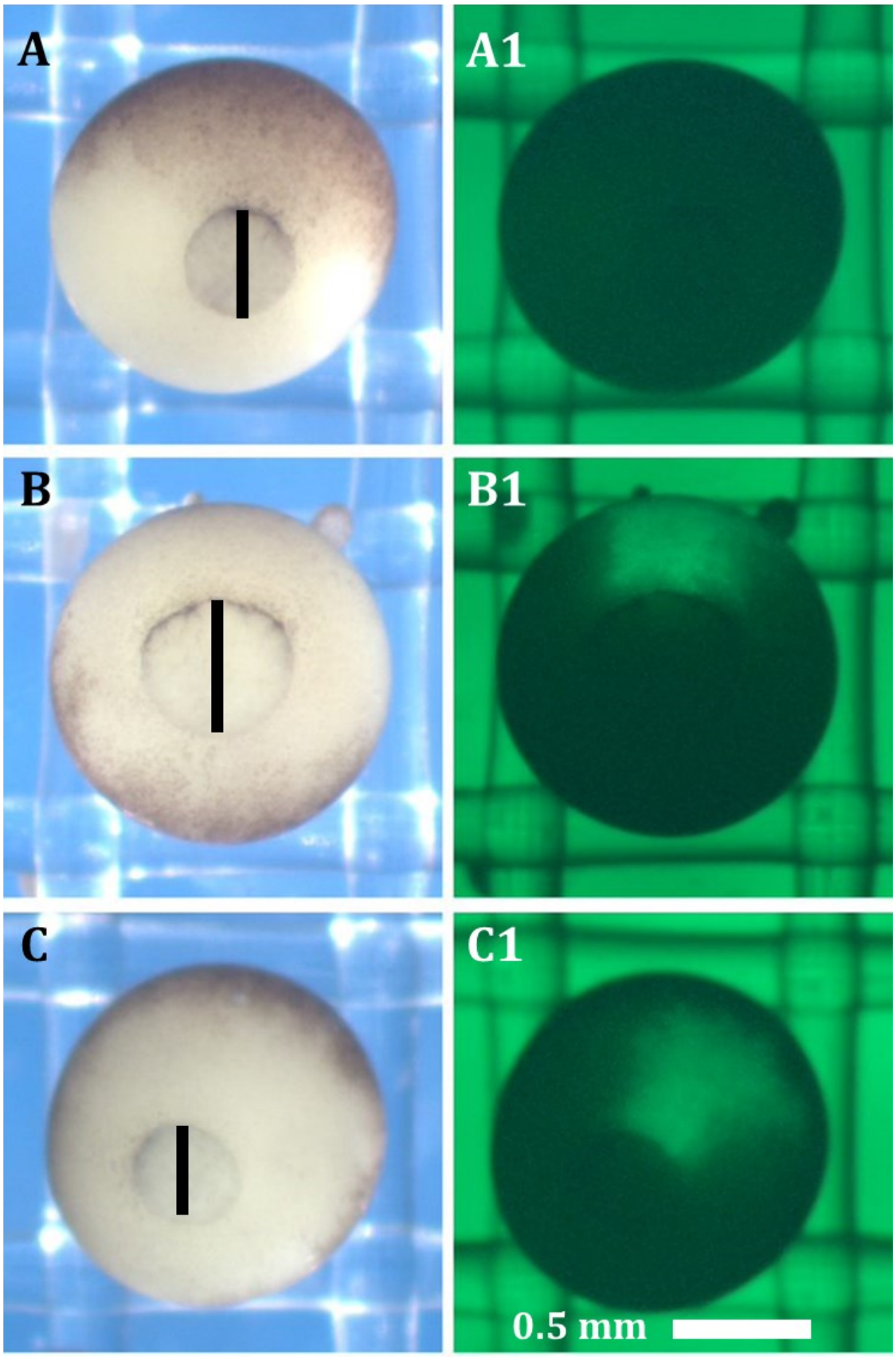
A
A1
B
B1
C
C1
0.5 mm

Figure 3.9 Overexpression of GFP tag and full-length α-parvin does not delay blastopore closure during *Xenopus* gastrulation. Embryos were injected in the future dorsal side at stage 2 with mRNA representing GFP or GFP-FLAP in equimolar ratios. Blastopore closure was imaged at stage 11.5 (A-C). GFP expression is visualized on the right side of embryos (A1-C1). Control uninjected (A), GFP (B) and FLAP (C) expressing embryos show normal progression of blastopore closure. Black bars span the blastopore diameter.

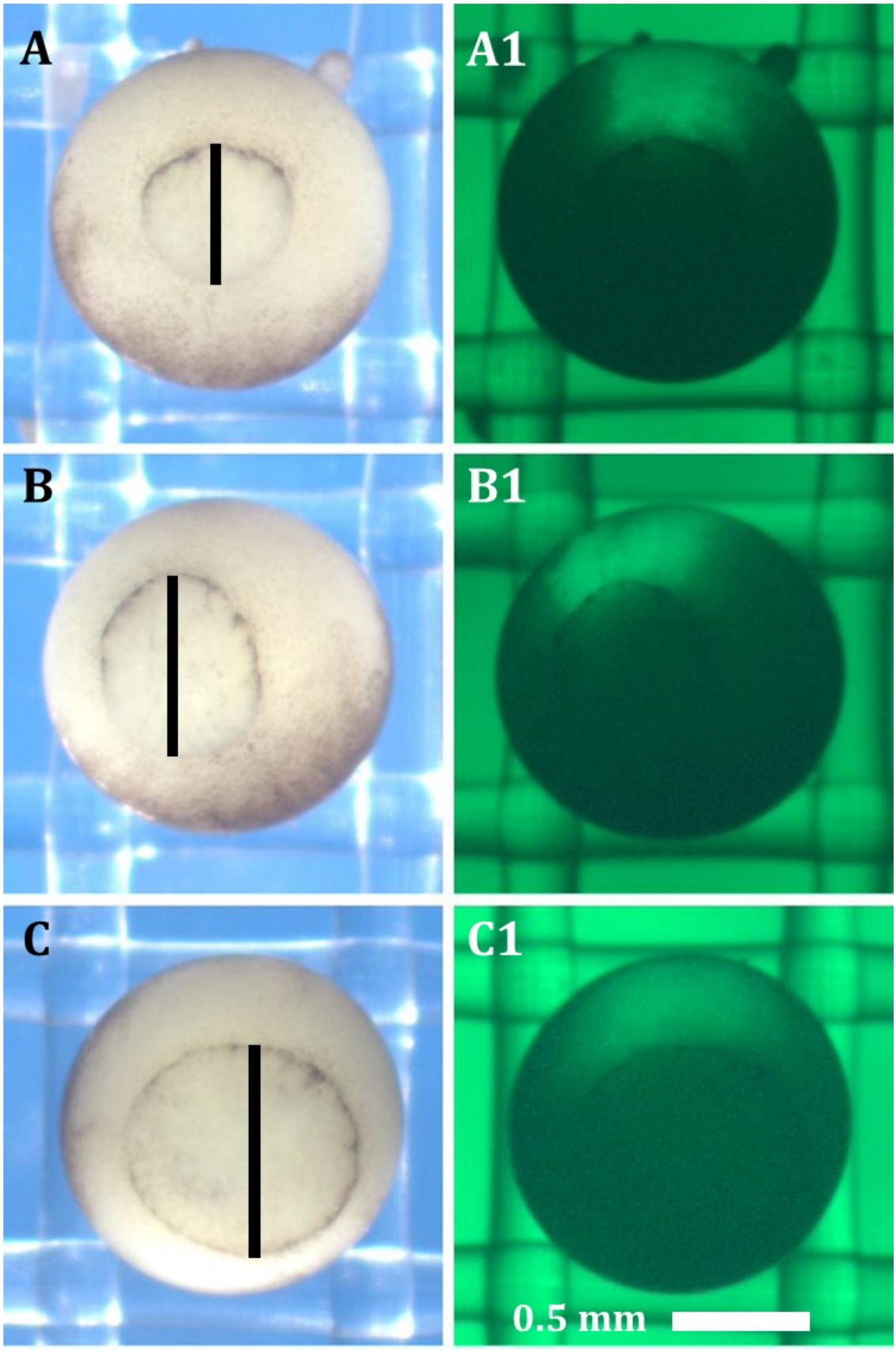
A
A1
B
B1
C
C1
0.5 mm

Figure 3.10 Over-expression of RP1 and RP2 delays blastopore closure during *Xenopus* gastrulation. Embryos were injected in the future dorsal side at stage 2 with mRNA representing GFP, GFP-RP1, or GFP-RP2 in equimolar ratios. Blastopore closure was imaged at stage 11.5 (A-C). GFP expression is visualized on the right side of embryos (A1-C1). RP1 (B) and RP2 (C) over-expressing embryos exhibit delays in blastopore closure compared to GFP (A) embryos. Black bars span the blastopore diameter.

3.5.2 CH1 and CH2 domains of α-parvin interfere with tissue rearrangements during gastrulation

During gastrulation, the ectoderm, mesoderm, and endoderm tissues undergo extensive rearrangements. In *Xenopus* embryos, the involuting mesoderm attaches to the blastocoel roof and extends towards the future anterior. The extending mesoderm drags endoderm and creates a cavity in its wake called the archenteron. The archenteron grows in length and size as the mesoderm extends anterior and displaces the blastocoel. It is well described that disrupting integrin disrupts mesoderm extension in *Xenopus* (Rozario et al., 2009), so I asked if over-expressing my constructs would affect the internal tissue architecture of gastrulating *Xenopus* embryos.

Embryos were injected at the two-cell stage in the future dorsal side with mRNA representing GFP, FLAP, RP1 and RP2 in equimolar ratios and cultured until stage 11.5. GFP expression was confirmed, and embryos were fixed. The embryos were bisected along the sagittal plane and phenotypes were recorded (Figure 3.11, A-C; Figure 3.12, A-C). It should be noted that TCA destroys GFP fluorescence and therefore GFP cannot be imaged in these embryos post-fixation. The three germ layers; mesoderm (red), endoderm (yellow) and ectoderm (blue), are colored to illustrate the interior tissue layout (Figure 3.11, Panel A1-C1; Figure 3.12, Panel A1-C1). These represent the bulk arrangement of the primary germ layers and smaller details are not included in these cartoons. Control uninjected embryos exhibit a normal internal tissue arrangement expected of *Xenopus* gastrulae (Figure 3.11, Panel A, A1). The mesoderm extends completely to the anterior end of the embryo (upper red) and a large archenteron (A) is present (Figure 3.11, Panel A1). The

blastocoel (B) is being forced anterior and ventral while decreasing in volume. Injection of GFP mRNA results in similar phenotypes to the controls (Figure 3.11, Panel B). Over-expression of GFP-FLAP in embryos also results in no noticeable changes in phenotype compared to the controls (Figure 3.11, Panel C). By comparison, over-expression of GFP-RP1 and GFP-RP2 cause significant defects in mesoderm migration and archenteron formation (Figure 3.12, Panel A-C). The internal tissue architecture of GFP-RP1 injected embryos is disorganized (Figure 3.12, Panel B). In comparison to GFP expressing embryos, the archenteron (A) is diminished in size and length (Figure 3.12, Panel B1). In addition, the dorsal mesoderm (red) has not extended wholly to the anterior end (Figure 3.12, Panel B1). The blastocoel (B) has not displaced ventrally, and the endoderm is disorganized and fragmented. GFP-RP2 injected embryos also exhibit defects in internal architecture (Figure 3.12, Panel C). The mesoderm (upper red) does not extend as far as observed in control embryos but appears to be longer than that observed in the RP1 over–expressing embryos. The archenteron is also significantly shortened in size and length compared to GFP injected embryos (Figure 3.12, Panel C1). Uniquely, the mesoderm (upper red) in GFP-RP2 injected embryos is detached from the blastocoel roof (white arrow) (Figure 3.12, Panel C1). The blastocoel (B) is expansive and irregular in shape being displaced more centrally. The cells that make up the endoderm are loose and do not form a coherent tissue. Unlike their exterior phenotype (Figure 3.10), the internal defects of gastrulating embryos overexpressing GFP-RP1 and GFP-RP2 are disparate (Figure 3.12) suggesting unique mechanisms are responsible.

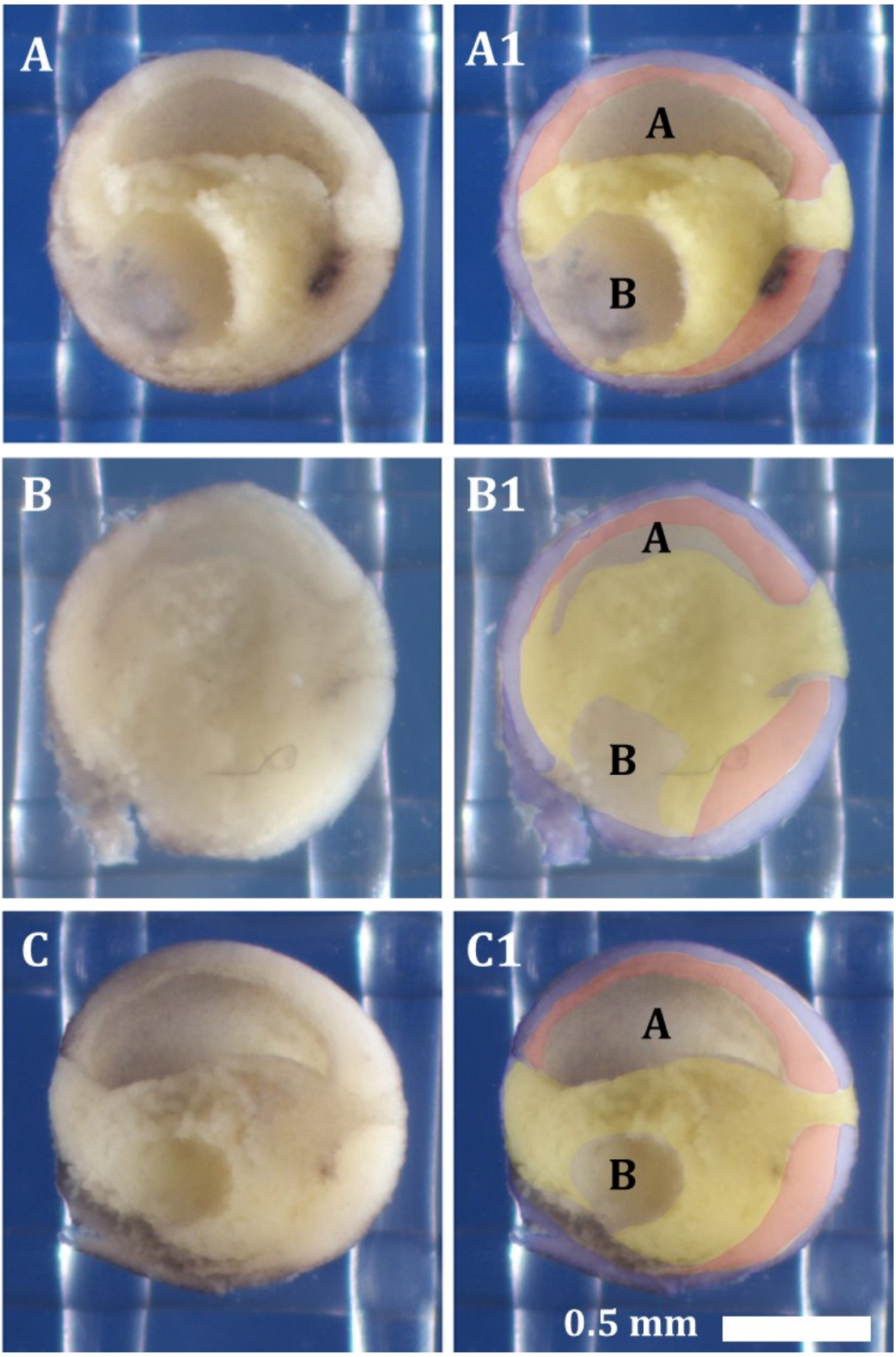
A
A1
A
B
B
B1
A
B
C
C1
A
B
0.5 mm

Figure 3.11 Overexpression of GFP and full-length α-parvin does not inhibit mesoderm extension during gastrulation. Embryos were injected in the future dorsal side of stage 2 embryos with mRNA representing GFP or GFP-FLAP in equimolar ratios. Embryos were cultured until stage 12, bisected along the sagittal plane, and imaged (A-C). The mesoderm (red), endoderm (yellow), and ectoderm (blue) are illustrated in panels on the right (A1-C1). The archenteron (A) and blastocoels (B) are regular. Control uninjected (A), GFP (B) and FLAP (C) expressing embryos show normal mesoderm extension to the anterior end and archenteron formation, displacing the blastocoel.

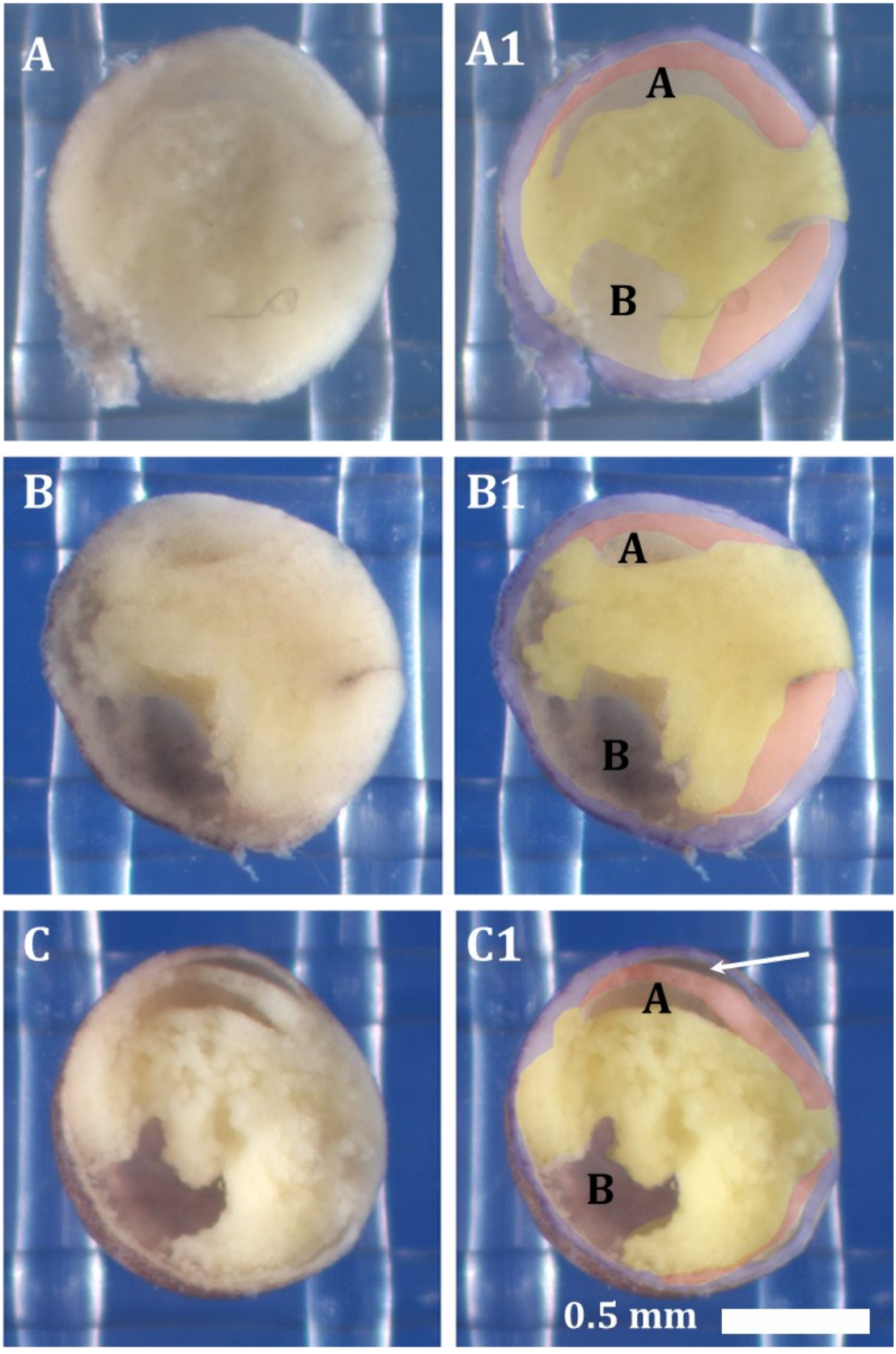
A
A1
A
B
B
B1
A
B
C
C1
A
B
0.5 mm

Figure 3.12 Overexpression of RP1 and RP2 inhibits mesoderm extension during gastrulation. Embryos were injected in the future dorsal side of stage 2 embryos with mRNA representing GFP, GFP-RP1, or GFP-RP2 in equimolar ratios. Embryos were cultured until stage 11.5, bisected along the sagittal plane, and imaged (A-C). The mesoderm (red), endoderm (yellow), and ectoderm (blue) are illustrated in panels on the right (A1-C1). GFP (A) expressing embryos display normal mesoderm extension and archenteron formation. RP1 (B) expressing embryos exhibit a disorganized tissue interior, diminished archenteron (A), and disrupted mesoderm extension. The blastocoel (B) is not displaced ventrally. RP2 (C) expressing embryos exhibit a reduced archenteron (A), disrupted mesoderm extension, and mesoderm detachment from the blastocoel roof (arrow). The blastocoel (B) is expansive and displacing more centrally.

3.5.3 CH1 and CH2 disrupt the anterior-posterior axis

Xenopus embryos undergo neurulation at developmental stage 17. Neurulation is the developmental process that immediately follows gastrulation. As such, defects at this stage may be the result of failures in neurulation or may be downstream of gastrulation defects. To observe the effects of my over-expressed constructs downstream of gastrulation, I compared the phenotypes of stage 17 embryos.

Embryos were injected with mRNAs that represent GFP, GFP-FLAP, GFP-RP1 and GFP-RP2 at the two-cell stage in the future dorsal side in equimolar ratios and cultured until stage 17. GFP expression was confirmed (Figure 3.13, Panel A1-C1; Figure 3.14, Panel A1-C1), and phenotypes were recorded (Figure 3.13, Panel A-C; Figure 3.14, Panel A-C). Control uninjected embryos (Figure 3.13, Panel A) have a neural tube that extends along the anterior-posterior axis. The anterior end features an open anterior neuropore (arrow). As expected, there is no GFP expression in the controls (Figure 3.13, Panel A1). Over-expression of GFP (Figure 3.13, Panel B, B1) results in phenotypes similar to the controls (Figure 3.13, Panel B). GFP-FLAP over-expression also produces no change in phenotype (Figure 3.13, Panel C), having a neural tube that extends the full length of the embryo (Figure 3.13, Panel B-C). GFP expression reveals proper convergence in the mesoderm and an extended anterior-posterior axis (Figure 3.13, Panel B1-C1). In contrast, over-expression of GFP-RP1 and GFP-RP2 causes disruption to the anterior-posterior axis and defects in the neural plate when compared to embryos expressing GFP alone (Figure 3.14, Panel B-C). Embryos over-expressing GFP-RP1 feature a short anterior-posterior axis and severe disruptions to anterior tissues. The GFP expressing tissue takes on a distinctive

swirling pattern and there is no clear convergence of the more posterior tissue (Figure 3.14, Panel B). In many GFP-RP1 expressing embryos, the defects were severe enough that the dorsal neural plate was unrecognizable. Surprisingly, these embryos often recover and develop into tadpoles (Figure 3.16). The GFP-RP2 injected embryos have open neuropores (black arrow) at the anterior end and frequently, open blastopores (white arrow) at the posterior end (Figure 3.14, Panel C). These embryos also possess a short anterior-posterior axis and are bent (Figure 3.14, Panel C). GFP expression in these embryos reveals the tissue has not undergone complete convergent extension and remains a broad strip along the embryo (Figure 3.14, Panel C1). The embryo phenotypes in embryos over-expressing GFP-RP1 and GFP-RP2 are distinct at stage 17.

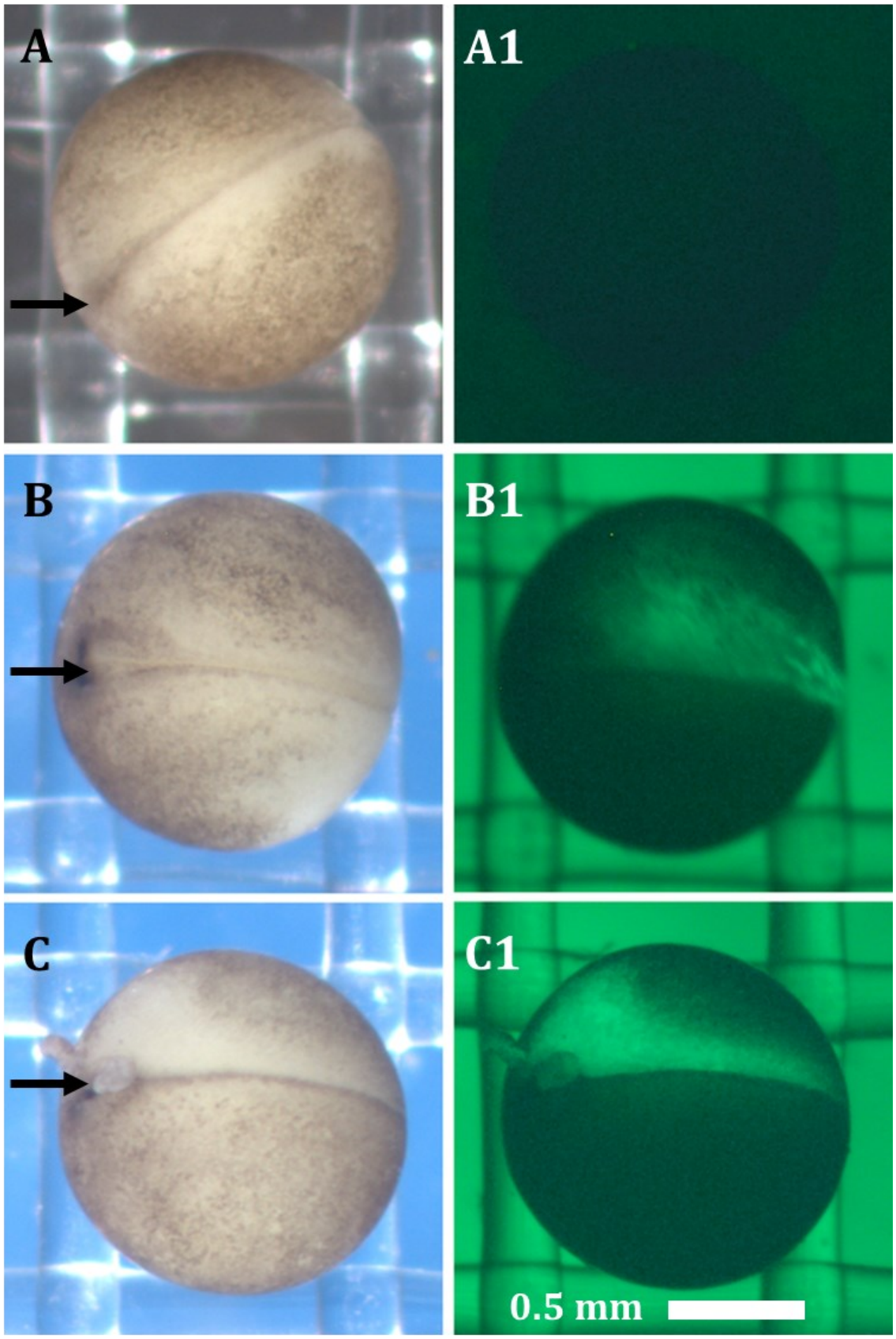
A
A1
B
B1
C
C1
0.5 mm

Figure 3.13 Overexpression of GFP and full-length α-parvin does not disrupt the anterior-posterior axis. Embryos were injected in the future dorsal side of stage 2 embryos with mRNA representing GFP and GFP-FLAP in equimolar ratios. Embryos were cultured until stage 17 and imaged (A-C). GFP expression is visualized to the right side of embryos (A1-C1). Control uninjected (A), GFP (B) and FLAP (C) expressing embryos show normal developmental phenotypes. These embryos have a neural tube that extends the full length of the embryo, open neuropore (arrow), and an extended anterior-posterior axis.

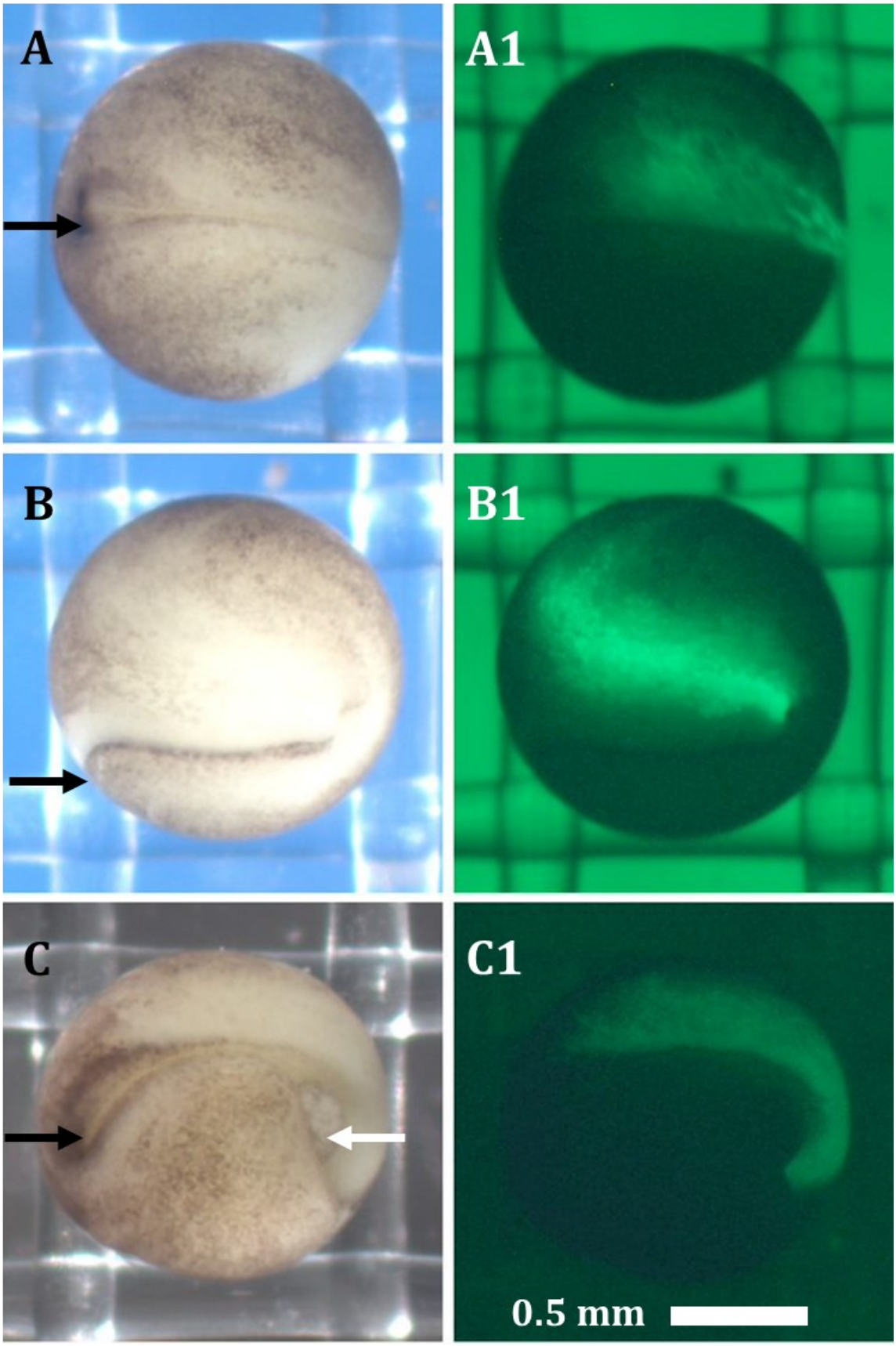
A
A1
B
B1
C
C1
0.5 mm

Figure 3.14 Overexpression of RP1 and RP2 disrupts the anterior-posterior axis. Embryos were injected in the future dorsal side of stage 2 embryos with mRNA representing GFP, GFP-RP1, or GFP-RP2 in equimolar ratios. Embryos were cultured until stage 17 and imaged (A-C). GFP expression is visualized to the right side of embryos (A1-C1). GFP (A) expressing embryos have a neural tube that extends the full length of the embryo and an extended anterior-posterior axis. RP1 (B) expressing embryos exhibit a short anterior-posterior axis and severe disruptions to anterior tissues. GFP expression takes on a swirling pattern and there is no clear convergence of the more posterior tissue (B1). RP2 (C) expressing embryos have open neuropores (black arrow) at the anterior end and open blastopores (white arrow) at the posterior end. These embryos also feature a short anterior-posterior axis and are greatly bent. GFP (C1) expression reveals the tissue has not undergone convergent extension and remains a broad strip along the embryo.

3.5.4 Tadpoles exhibit downstream defects of CH1 and CH2 disruption during gastrulation

Embryos were injected at stage 2 in the future dorsal side with mRNA representing GFP, FLAP, RP1 and RP2 in equimolar ratios and cultured until stage 28. Phenotypes were recorded and compared (Figure 3.15, Panel A-C; Figure 3.16, Panel A-C). Tadpole stage embryos are motile and to collect images, the embryos are fixed. This destroys the GFP and as such it is not possible to collect images of GFP expression. Embryos were checked for GFP expression prior to fixation. Control uninjected tadpoles demonstrate phenotypes expected of normal growth. In these embryos, the cement gland is present and the anterior-posterior axis has extended. The head is well developed with eyes and the tail is extending in the posterior. (Figure 3.15, Panel A). Over-expression of the GFP-tag does not induce observable defects and embryos appear similar to the controls (Figure 3.15, Panel B). GFP-FLAP injected embryos exhibit an arched anterior-posterior axis, but overall morphology is normal. There is a distinct head with eyes, a cement gland, and a developing tail (Figure 3.15, Panel C). GFP-RP1 injected tadpoles have a kink just posterior to the head, sharply bending the head posterior (black arrows). These embryos demonstrate anterior-posterior axial truncation compared to GFP injected embryos (Figure 3.16, Panel A-B). On average, GFP injected embryos are approximately 3.1 mm in length, while GFP-RP1 injected embryos are approximately 2.7 mm in length, demonstrating an 12.9% difference in axis length. Most interestingly, the GFP-RP1 expressing embryos have protrusions that lie along the flanks of the tadpole (Figure 3.16, Panel B, orange arrows). These protrusions resemble a second axis, although this has not been confirmed. RP2 injected tadpoles demonstrated an array of defects (Figure 3.16, Panel C). Tadpoles over-expressing GFP-RP2

are hunched along the anterior-posterior axis (Figure 3.16, Panel B-C). These hunches arc in the opposite direction and are longer and shallower when compared to the sharp kinks found in RP1 expressing tadpoles. The majority of the tadpoles possessed retained blastocoels which cause blisters on the belly of the embryo (Figure 3.16, Panel C, yellow arrow). GFP-RP2 injected embryos are shorter (2.4 mm) when compared to GFP-RP1 (2.7 mm) and GFP (3.1 mm) injected embryos (Figure 3.16, Panel, A-C). The defects seen in RP1 expressing stage 28 tadpoles are distinct from those expressing GFP-RP2, further reinforcing that the two isolated CH domains are acting on independent pathways.

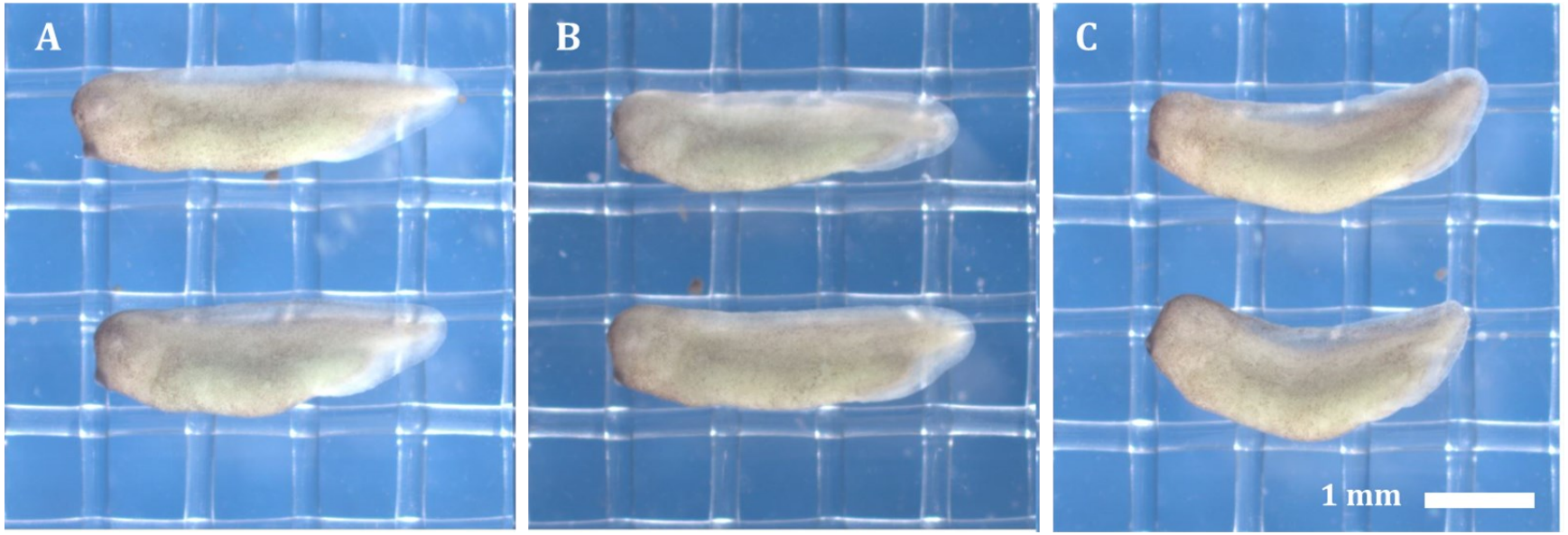

Figure 3.15 Overexpression of GFP and full-length α-parvin does not cause major defects at organogenesis. Embryos were injected in the future dorsal side of stage 2 embryos with mRNA representing GFP and GFP-FLAP in equimolar ratios. Embryos were cultured until stage 28 and imaged (A-C). Control uninjected (A) and GFP (B) expressing embryos show normal developmental phenotypes. These embryos have an extended anterior-posterior axis and features of normal growth including developing tail, head, eyes, and a cement gland. FLAP (C) expressing embryos exhibit a slightly arched anterior-posterior axis.

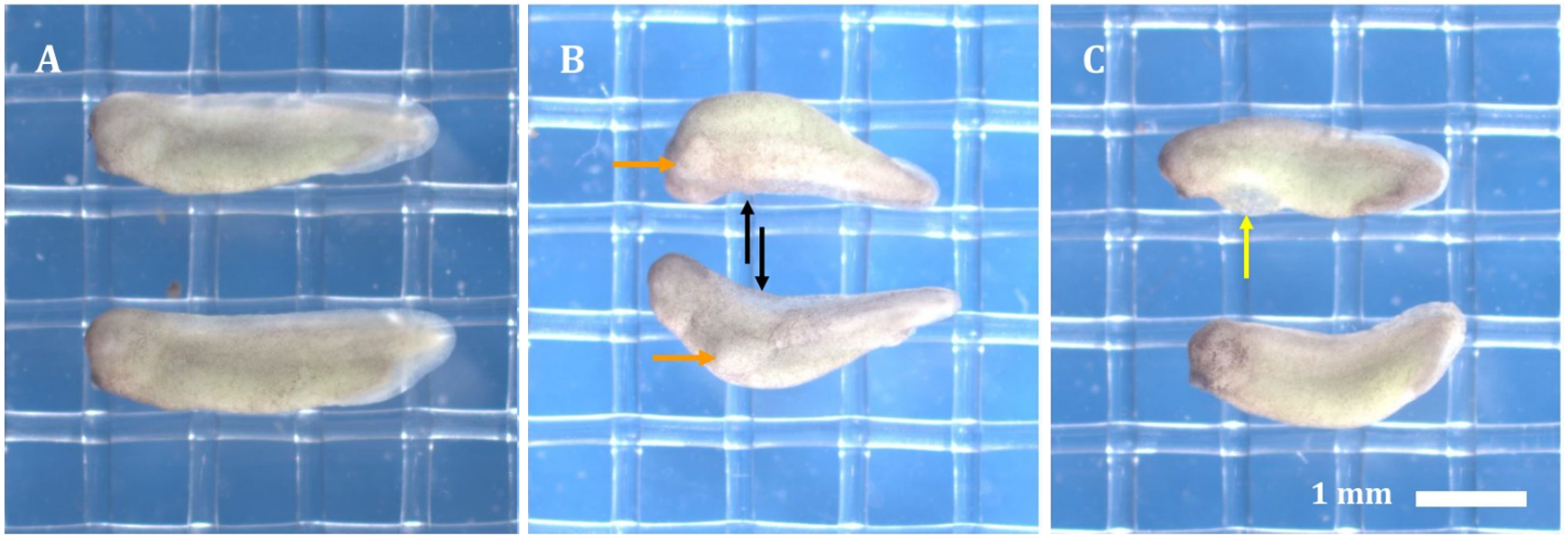

Figure 3.16 Overexpression of RP1 and RP2 cause major defects at organogenesis. Embryos were injected in the future dorsal side of stage 2 embryos with mRNA representing GFP, GFP-RP1, and GFP-RP2 in equimolar ratios. Embryos were cultured until stage 28 and imaged (A-C). GFP (A) expressing embryos show normal developmental phenotypes such as a cement gland and eyes. These embryos also display an extended anterior-posterior axis and both a developing tail and head. RP1 (B) expressing embryos feature a large kink (black arrows) in the anterior-posterior axis and a protrusion that resembles a second axis (orange arrows). These embryos also display slight anterior-posterior axial truncations. RP2 (C) expressing embryos demonstrate an arched anterior-posterior axis and some retained blastocoel belly blisters (yellow arrow). These embryos also exhibit anterior-posterior axial truncations.

4.0 Discussion

4.1 Cloning and sequence analysis of *Xenopus* α-parvin

I have characterized and made a preliminary study on the function of α-parvin in *Xenopus laevis*. I searched *Xenbase* (*Xenbase*: Karimi et al., 2018) for genomic data representing an α-parvin ortholog in *Xenopus*. This genomic data was used to design primers used in RT-PCR to generate a cDNA representing *Xenopus* α-parvin. *Xenopus* α-parvin was successfully cloned and the amino acid sequence revealed features common to other known α-parvin proteins (Figure 3.1). These include the two conserved calponin-homology (CH) domains separated by a 60 amino acid linker sequence. Analysis of the amino acid sequence revealed a high degree of identity with human (94%), murine (92%), chicken (93%), and zebrafish (87%) α-parvin orthologs (Figure 3.2). *Xenopus* α-parvin shares higher identity with other α-parvin orthologs than with *Xenopus* β-parvin (Figure 3.3) and suggesting the cDNA I retrieved represents a true *Xenopus* α-parvin.

The highest conservation of amino acid sequence is in the two CH domains. In the CH1 domain, there is only a single amino acid that differs between mammals to *Xenopus* (amino acid 138). In the CH2 domain, there are two amino acids that differ between mammals and *Xenopus* (amino acids 311 & 312). Since the CH domains mediate protein-protein interactions, this remarkable sequence identity suggests that the binding partners of α-parvin CH1 and CH2 domains are also conserved. This means that discoveries made in *Xenopus* are likely applicable across many species.

α-parvin is a member of the parvin family, which contains α-, β-, and y-parvin. In mammals these paralogs are encoded by distinct genes (Tu et al., 2001; Olski et al., 2001; Yamaji et al., 2001). *Drosophila* and other invertebrates, on the other hand, possess only a single parvin ortholog. Pair-wise amino acid sequence alignments reveal that *Drosophila melanogaster* shares the least similarity with the other α-parvin orthologs (53%, Figure 3.2). Most interestingly, *Drosophila* parvin shares higher identity with β-parvin orthologs than α-parvin orthologs (Figure 4.1). These observations combined suggests that the invertebrate parvin ortholog likely represents a more ancestral parvin. Furthermore, this data also suggests that in vertebrates, β-parvin represents the ancestral gene, and that α-parvin evolved more recently through a duplication event.

The *Xenopus laevis* genome on *Xenbase* was described by Session et al., in 2016. The genomic data comes from the inbred 'J' strain of *Xenopus* (Session et al., 2016). While the 'J' strain was used for more consistent genomic data, it has a smaller genome than outbred strains. One of the difficulties in using *Xenopus* as a model organism is that most labs use wild caught or outbred commercial stocks. Therefore, the genomic data on *Xenbase* is not always congruous with lab isolated cDNAs. Despite that, the conservation between my isolated α-parvin cDNA and the genomic data is very high (99.5% identity to Genbank accession# XP_018112776).

Xenopus laevis is an allotetraploid organism, evolving from a hybridization event ~17 million years ago (Session et al., 2016). The two resultant subgenomes, 'L(ong)' and 'S(hort)', are not symmetrical, with differences in both structure and gene expression. RNA-seq data of α-parvin suggests the expression levels of the 'L' homolog are higher than the 'S'

homolog throughout *Xenopus* development (*Xenbase*: Karimi et al., 2018, Session et al., 2016). Differences in α-parvin transcript expression peaks at stage 9 where the 'L' homolog (36.4 transcripts per million (TPM)) is expressed ~4x more than the 'S' homolog (9.3 TPM) (*Xenbase*: Karimi et al., 2018, Session et al., 2016). Therefore, the primers used to generate α-parvin cDNA were designed to 'L' α-parvin (Table 2.1). The differences between the 'L' and 'S' homologs of α-parvin are minimal. The two nucleotide sequences share 95.6% similarity and differences are isolated and non-sequential. The primers used in experiments cover only two nucleotide differences, but due to the location of these changes, this is likely not enough to distinguish the 'L' and 'S' homologs when I use these primers in PCR. However, the amino acid sequence of the 'L' and 'S' homologs of α-parvin share 99.46% identity with only 2 amino acid differences. Therefore, while the primers I used may not distinguish between the 'L' and 'S' homologs of α-parvin, both genomes encode essentially functionally identical proteins.

4.2 α-parvin expression is increased during gastrulation

RNA-seq data on *Xenbase* (Karimi et al., 2018, Session et al., 2016) indicate peak level of α-parvin transcripts at stage 9 just before the onset of gastrulation. I assessed the temporal expression of the α-parvin cDNA that I isolated throughout embryogenesis using RT-PCR (Figure 3.4). Multiple trials reveal a consistent pattern of increased α-parvin expression at stage 10 and 11. α-parvin mRNA is initially expressed maternally and then zygotically post mid-blastula transition (Stage 7). In *Xenopus*, the complete genome is expressed maternally, even if the proteins encoded by these maternal mRNAs are not used in early development. For proteins that are required during gastrulation it is common to see a pattern where there is high mRNA prevalence that decreases leading up to gastrulation. Then zygotic expression drives a peak accumulation close to stage 10. The increase in α-parvin mRNA expression during development stages correlating to gastrulation suggests α-parvin plays a role in *Xenopus* gastrulation. Over multiple trials my results were not always completely consistent. PCR is complex and there are multiple potential sources of error. There is an assumption that the cDNA synthesis reactions produce equal yields across different samples. There is no control for the efficiency of RT-PCR and by using a set percentage of the cDNA synthesis volume in the subsequent PCR, it is possible the results include variability. Therefore, in my experiments, temporal expression data (Figure 3.4) should be viewed as qualitative and not quantitative. Despite the above limitations it is clear that α-parvin is expressed during *Xenopus* gastrulation.

4.3 α-parvin and CH2 compartmentalize to focal adhesions *in vitro*

There are several approaches to looking at the role a specific protein plays in development. The most powerful is to use an RNAi approach to degrade or inhibit the translation of specific mRNAs eliminating protein expression. This is not possible in *Xenopus* as embryos contain an unwindase activity that prevents RNA-RNA duplexes. (Wagner et al., 1989). Most *Xenopus* research labs use morpholinos (a synthetic nucleotide analogue) to block mRNA translation. This approach has been powerful and revealing. However, to design morpholinos I require more sequence data than there is available. This is further complicated by the allotetraploid genome that could require two individual morpholinos. Therefore, for this preliminary examination of α-parvin, I used an over expression approach which is commonly used in *Xenopus*. My experiments follow a similar approach used to characterize β-parvin in *Xenopus* (Studholme, 2013) and therefore, I performed over-expression experiments. α-parvin is a scaffolding protein that interacts with binding partners through its two CH domains. I created constructs that isolate the CH1 (RP1) and CH2 (RP2) domains of α-parvin and compared the over-expression of these isolated domains to that of full-length α-parvin (FLAP).

I looked at α-parvin subcellular compartmentalization using cultured cell transfections (Figure 3.6). Both FLAP and RP2 are found in focal adhesions while the RP1 construct isolating CH1 remains mostly cytosolic or is found associated with actin stress fibers. Since the RP1 construct is not recruited to focal adhesions the CH2 domain found in FLAP and the RP2 construct is likely responsible for recruitment to focal adhesions. This recruitment is likely through the documented interactions between α-parvin and ILK (Tu et

al., 2001). My results correlate with previous mammalian studies where α-parvin and β-parvin are found to localize in focal adhesions and interact with ILK to form part of the IPP complex (Tu et al., 2001; Yamaji et al., 2001). ILK then recruits the complex to β1 and β3 integrin tails at sites of integrin adhesion (Zhang et al., 2002; Yamaji et al., 2001). The interactions mediated through the RP1 construct containing the CH1 domain are not well described. A previous analysis of the CH1 domain in α-parvin revealed it shared similarities with the CH1 domain of β-spectrin, which binds to F-actin. The CH1 domain of β-spectrin links F-actin to filament networks. Furthermore, when the CH1 domain of b β-spectrin is isolated or disrupted by mutation, it has a high affinity for actin (Avery et al., 2017). When I create the RP1 construct I am removing the highly structured CH2 domain, and it is possible this results in an increased affinity for filamentous actin by the now unconstrained CH1 domain. Such a scenario could explain why α-parvin CH1 is found with actin stress fibers in *Xenopus* A6 cells. In *Xenopus,* the β-parvin CH1 domain is not recruited to focal adhesions and instead localizes to sites of cell-cell adhesion mediated through C-cadherin (Studholme, 2013). The subcortical region at these sites of cell-cell adhesion is rich in filamentous actin and it may well be that the CH1 domain is localizing to actin rich structures. While the binding partner for the α-parvin CH1 domains remains unclear, these observations clearly lay out unique functions for the individual CH domains.

α-parvin and β-parvin both localize to focal adhesions in mammalian cells through interactions with ILK. In HeLa cells, their interaction with ILK is mutually exclusive and appears to be antagonistic (Yamaji et al., 2001; Tu et al., 2001; Zhang et al., 2004). To test if this antagonistic relationship exists in *Xenopus*, I co-transfected α-parvin and β-parvin constructs into *Xenopus* A6 cells (Figure 3.7). α-parvin and β-parvin co-localize to the same

focal adhesions. However, they sometimes compartmentalize exclusively. Suggesting that in *Xenopus*, at least, α-parvin and β-parvin are not mutually exclusive. In cell adhesion assays, mutations disrupting CH2-ILK binding in α-parvin significantly reduced cell adhesion (Tu et al., 2001). This suggests α-parvin plays a positive role in regulating cell adhesion. Interestingly, knockdown of α-parvin induced lamellipodia formation and cell-spreading in HeLa cells (Fukuda et al., 2003). It is possible that these observations are promoted by β-parvin in the absence of α-parvin, due to their antagonistic relationship (Fukuda et al., 2003; Zhang et al., 2004). This is supported by evidence that β-parvin and ILK are found in the leading edge of lamellipodia where *de novo* focal adhesions are forming (Yamaji et al., 2001). These observations provide a potential model for the exclusive compartmentalization of α-parvin and β-parvin, where β-parvin is actively recruited to nascent sites of focal adhesion and α-parvin remains in stable focal adhesions as a regulator of cell adhesion. My results reveal a co-localization of α-parvin and β-parvin in the same focal adhesion. Despite being in the same adhesion site, the localization is not always overlapping; with the two parvins occupying distinct zones within the adhesion (Figure 3.7). Focal adhesions are highly dynamic structures, forming and maturing before turning over in migrating cells (reviewed Webb et al., 2002; Broussard et al., 2008). It is possible that when I am seeing two parvins in the same focal adhesion I am seeing the turnover of that adhesion site. This could be confirmed with higher resolution experiments that look at protein turn over in focal adhesions. This has been done in cultured cells using photobleaching approaches as well as recording the formation and turnover of focal adhesions in motile cells (reviewed in Webb et al., 2002).

4.4 Functional analysis of α-parvin CH domains during *Xenopus* embryogenesis

Since the constructs localized as expected they could now be used in embryo experiments. I decided to perform my injections at a concentration of FLAP that would have minimal disruption to normal development. This would allow me to gauge the effects of the isolated CH domains versus the complete molecule. Once I titred FLAP, I tested if injecting equimolar ratios of my constructs would induce defects (Figure 3.8). By the tadpole stage a small percentage (13%) of FLAP expressing embryos showed phenotypes that can be attributed to minor errors occurring during gastrulation. While the percentage of embryos showing defects is higher than that observed in GFP expressing embryos (5.3%) and controls (6.3%), the defects themselves are minor and these embryos produce normal looking swimming tadpoles (data not shown). On the other hand, embryos over expressing the isolated CH domains show profound developmental defects. 93% of embryos over-expressing the CH1 domain and 75% of embryos over expressing the CH2 domain exhibit defects (Figure 3.8). This indicates that when isolated, the individual CH domains can interfere with normal parvin function likely through the saturation of binding partners. However, overexpression of FLAP does not cause significant embryonic defects suggesting that these phenotypes may also arise from defects caused by the CH domains no longer being associated within a single molecule. This is supported by evidence in β-parvin that co-expression of the CH1 and CH2 domains cannot rescue normal parvin function and instead cause more significant defects (Studholme, 2013).

4.4.1 The isolated CH1 domain of α-parvin causes developmental defects

Over-expression of the RP1 containing the CH1 domain inhibits blastopore closure (Figure 3.9), the same phenotype that was observed in β-parvin RP1 construct over-expression (Studholme, 2013). CH1 over-expression also causes severe disruption to internal tissue rearrangements (Figure 3.12). Mesoderm extension to the anterior end is disrupted and as a result the archenteron is diminished in size and length. Downstream of gastrulation, the RP1 construct disrupts anterior tissues and dorsal neural plate structure (Figure 3.14). There is no clear convergence of the posterior tissue, and the anterior-posterior axis is truncated. By stage 28, the tadpole head is kinked, characteristic of defects where the notochord does not extend into the head (Figure 3.16). All these defects are indicative of failure in convergent extension in the axial mesoderm. Although these phenotypes are resemblant of disruption to α5β1 integrin adhesion to FN, it is unlikely that the CH1 domain is playing a direct role in integrin adhesion as CH1 does not localize to sites of integrin adhesion (Figure 3.6). In β-parvin, the CH1 domain inhibits FN matrix assembly, despite no disruption to integrin-FN ligation (Studholme, 2013). Instead, the β-parvin CH1 domain modulates cellular behaviour in involuted mesoderm by influencing the Rac1 pathway (Studholme, 2013). This could suggest an avenue for failure in convergent extension without direct disruption to α5β1 integrin adhesion to FN. However, the CH1 domain of α-parvin and β-parvin are not likely to exert their influence through the same binding partners. As such, additional testing is required to determine potential binding partners for the α-parvin CH1 domain.

The tadpoles over expressing the CH1 domain exhibit a protrusion that resembles a duplicate axis (Figure 3.16). It is possible that over-expression of the CH1 domain has split the normal axis. The formation of anterior-posterior axis in *Xenopus* is well described and requires the accumulation of β-catenin on the dorsal side of the embryo post fertilization (Schneider et al., 1996). Experiments that manipulate the accumulation of β-catenin in the ventral side of the embryo are known to produce a second axis (McCrea et al., 1993; Funayama et al., 1995). In the sea urchin embryo, expression of cadherin tails can act as a dominant negative to sequester β-catenin and alter developmental pathways (Logan et al., 1999). Interestingly, while the parvins are integrin associated molecules they have also been described to have interactions with cadherin (Olski et al., 2001). In *Xenopus*, recent evidence suggests that β-parvin CH1 domain can interact with the cytoplasmic tail of C-cadherin (Knapp, 2018) and possibly with β-catenin. This provides an avenue of investigation to examine if the isolated CH1 domain could play a role in the accumulation of β-catenin and allowing for a second ectopic axis. The caveat to these speculations is that I have not confirmed that the protrusions observed truly represent a second axis.

4.4.2 The CH2 domain of α-parvin affects integrin adhesion

The RP2 construct containing the CH2 domain inhibits blastopore closure (Figure 3.10). Interior views of the gastrula (Figure 3.12), reveals loose cells that makeup a disorganized endoderm and both mesoderm extension to the anterior end and archenteron formation are disrupted. (Figure 3.12). The blastocoel is irregularly shaped, and the mesoderm is detached from the blastocoel roof (Figure 3.12). This phenotype was also observed when the CH2 domain of β-parvin is over expressed (Studholme, 2013). Over

expression of the CH2 domain of β-parvin causes defects that closely resemble those associated with changes in integrin ligation to FN (Marsden & DeSimone, 2001). FN ligation to a5β1 integrin is required for both epiboly, convergent extension, and mesoderm attachment to the blastocoel roof (Marsden & DeSimone, 2001). β-parvin binds ILK through the CH2 domain and when the isolated CH2 domain is over expressed, it inhibits integrin mediated adhesion and FN assembly (Studholme, 2013). Since α-parvin is also known to bind ILK through the CH2 domain (Tu et al., 2001), it is likely that the CH2 domain is causing defects through a similar mechanism. Since both α-parvin and β-parvin bind ILK, it is expected that the over expressed CH2 domain of both molecules would result in similar phenotypes. This needs to be tested by investigating the effects of α-parvin CH2 domain over-expression on integrin adhesion.

In neurula, the blastopore remains open, and GFP expression indicates incomplete convergent extension of underlying tissue (Figure 3.14). This is what one would expect if integrin adhesion has been disrupted (Marsden & DeSimone, 2003). In tadpoles, the anterior-posterior axis is severely truncated and hunched (Figure 3.16). These neural and tadpole defects are likely not primary defects caused by CH2. Instead, it is likely these defects are downstream of disruption of integrin-FN ligation during gastrulation that prevents the proper rearrangement of the three primary germ layers (Marsden & DeSimone, 2001). Thus, I predict that the over-expressed CH2 domain acts to disrupt cell adhesion through interactions with ILK, but these assumptions require additional testing (section 4.6).

4.5 Conclusion

I successfully cloned *Xenopus* α-parvin and produced preliminary data to describe a potential mechanistic role. My data suggests that α-parvin plays an important role as a scaffolding protein through its CH domains during gastrulation. α-parvin likely affects integrin-mediated adhesion directly the CH2 domain. The CH1 domain produces different developmental defects and how it functions remains to be elucidated. Most interestingly, my data suggests a potential function for α-parvin in establishing a second axis through the CH1 domain.

4.6 Future Directions

My work presents a preliminary exploration of α-parvin function in *Xenopus laevis*. As such, my work has produced a number of questions that need to be answered before I can make conclusive statements on α-parvin function.

While I know α-parvin is expressed at all stages in development I was unable to determine the spatial localization of α-parvin in embryos. It is important to confirm where in the embryos α-parvin is expressed. As such, an in-situ hybridization would be the simplest approach. I made several attempts and could never produce conclusive results. My control experiments with other genes expressed during gastrulation worked well, indicating the technique was performed correctly. Future work in this area should concentrate on designing small probes with high melting temperatures that could be used in in-situ hybridizations. The possibility exists that α-parvin is not highly expressed, and as such, in-situ hybridizations would not be revealing. I was successful with a Xbra probe, but Xbra is expressed at a higher level than α-parvin (*Xenbase*: Karimi et al., 2018, Session et al.,

2016). This situation holds true for β-parvin as in-situ hybridizations produced indistinct faint colour reactions. An alternative is to produce an antibody against α-parvin to be used in whole mount immunocytochemistry. Given the high degree of conservation between α-parvin and β-parvin it may prove to be challenging to get an antibody that is α-parvin specific. This is reinforced by many of the commercially available antibodies not being able to distinguish between the two parvins.

While the embryo phenotypes give insights into the role that the CH1 and CH2 domains are performing, I have no data that directly supports a role for these molecules in cell adhesion. A cell adhesions assay describing embryonic cell adhesion similar to those in Studholme (2013) to both FN and cadherin should be done to help define roles for the two CH domains of α-parvin.

There is evidence of a potential second axis forming in RP1 expressing tadpoles but has yet to be confirmed. Observations of tadpoles that survive until stage ~50 show that these tadpoles do not generate a second head as is common for molecules that stabilize β-catenin. However, a few of these tadpoles did show duplications of the somites with a likely second notochord. This is suggestive that a true second axis is forming in these embryos. Confirmation of this would require sectioning of late gastrula through tadpole stage embryos. Experiments looking at β-catenin functions and interactions of the CH1 domain with cadherin would also provide much needed insights into my observations.

References

Avery, A. W., Fealey, M. E., Wang, F., Orlova, A., Thompson, A. R., Thomas, D. D., Hays, T. S., & Egelman, E. H. (2017). Structural basis for high-affinity actin binding revealed by a β-III-spectrin SCA5 missense mutation. *Nature Communications*, *8*(1). https://doi.org/10.1038/s41467-017-01367-w

Brieher, W. M., & Gumbiner, B. M. (1994). Regulation of C-cadherin function during activin induced morphogenesis of Xenopus animal caps. *Journal of Cell Biology*, *126*(2), 519–527. https://doi.org/10.1083/jcb.126.2.519

Broussard, J. A., Webb, D. J., & Kaverina, I. (2008). Asymmetric focal adhesion disassembly in motile cells. *Current Opinion in Cell Biology*, *20*(1), 85–90. https://doi.org/10.1016/j.ceb.2007.10.009

Clark, K. A., McGrail, M., & Beckerle, M. C. (2003). Analysis of PINCH function in Drosophila demonstrates its requirement in integrin-dependent cellular processes. *Development*, *130*(12), 2611–2621. https://doi.org/10.1242/dev.00492

Dagnino, L. (2011). Integrin-linked kinase: A Scaffold protein unique among its ilk. *Journal of Cell Communication and Signaling*, *5*(2), 81–83. https://doi.org/10.1007/s12079-011-0124-4

Davidson, L. A., Marsden, M., Keller, R., & DeSimone, D. W. (2006). Integrin α5β1 and Fibronectin Regulate Polarized Cell Protrusions Required for Xenopus Convergence and Extension. *Current Biology*, *16*(9), 833–844. https://doi.org/10.1016/j.cub.2006.03.038

Detrick, R. J., Dickey, D., & Kintner, C. R. (1990). The effects of N-cadherin misexpression on morphogenesis in xenopus embryos. *Neuron*, *4*(4), 493–506. https://doi.org/10.1016/0896-6273(90)90108-R

Dzamba, B.J., Bolton, M.A., DeSimone, D.W. (2001). The integrin family of cell

adhesion molecules. Cell Adhesion: Frontiers in Molecular Biology. Oxford, UK: Oxford University Press, 100-154.

Dzamba, B. J., Jakab, K. R., Marsden, M., Schwartz, M. A., & DeSimone, D. W. (2009). Cadherin Adhesion, Tissue Tension, and Noncanonical Wnt Signaling Regulate Fibronectin Matrix Organization. *Developmental Cell*, *16*(3), 421–432. https://doi.org/10.1016/j.devcel.2009.01.008

Fagotto, F. (2013). Looking beyond the Wnt pathway for the deep nature of β-catenin. *EMBO Reports*, *14*(5), 422–433. https://doi.org/10.1038/embor.2013.45

Fukuda, T., Chen, K., Shi, X., & Wu, C. (2003). PINCH-1 Is an Obligate Partner of Integrin-linked Kinase (ILK) Functioning in Cell Shape Modulation, Motility, and Survival. *Journal of Biological Chemistry*, *278*(51), 51324–51333. https://doi.org/10.1074/jbc.M309122200

Funayama, N., Fagotto, F., McCrea, P., & Gumbiner, B. M. (1995). Embryonic axis induction by the armadillo repeat domain of β-catenin: Evidence for intracellular signaling. *Journal of Cell Biology*, *128*(5), 959–968. https://doi.org/10.1083/jcb.128.5.959

Gahmberg, C. G., Fagerholm, S. C., Nurmi, S. M., Chavakis, T., Marchesan, S., & Grönholm, M. (2009). Regulation of integrin activity and signalling. *Biochimica et Biophysica Acta - General Subjects*, *1790*(6), 431–444. https://doi.org/10.1016/j.bbagen.2009.03.007

Ghil, J.-S., & Chung, H.-M. (1999). Evidence that Platelet derived growth factor (PDGF) action is required for mesoderm patterning in early amphibian (Xenopus laevis) embryogenesis. *International Journal of Developmental Biology*, *43*(4), 329–334.

Gimona, M., Djinovic-Carugo, K., Kranewitter, W. J., & Winder, S. J. (2002). Functional plasticity of CH domains. *FEBS Letters*, *513*(1), 98–106. https://doi.org/10.1016/S0014-5793(01)03240-9

Ginsberg, D., DeSimone, D., & Geiger, B. (1991). Expression of a novel cadherin (EP-cadherin) in unfertilized eggs and early Xenopus embryos. *Development*, *111*(2), 315–325.

Gumbiner, B. M. (2005). Regulation of cadherin-mediated adhesion in morphogenesis. *Nature Reviews Molecular Cell Biology*, *6*(8), 622–634. https://doi.org/10.1038/nrm1699

Gumbiner, B. M. (2000). Regulation of cadherin adhesive activity. *Journal of Cell Biology*, *148*(3), 399–403. https://doi.org/10.1083/jcb.148.3.399

Hannigan, G. E., Leung-Hagesteijn, C., Fitz-Gibbon, L., Coppolino, M. G., Radeva, G., Filmus, J., Bell, J. C., & Dedhar, S. (1996). Regulation of cell adhesion and anchorage-dependent growth by a new β1-integrin-linked protein kinase. *Nature*, *379*(6560), 91–96. https://doi.org/10.1038/379091a0

Hardin, J., & Keller, R. (1988). The behaviour and function of bottle cells during gastrulation of Xenopus laevis. *Development*, *103*(1), 211–230. https://doi.org/10.1242/dev.103.1.211

Hoffstrom, B. G. (2002). Integrin function during *Xenopus laevis* gastrulation. *Thesis. University of Virginia.*

Karimi, K., Fortriede, J. D., Lotay, V. S., Burns, K. A., Wang, D. Z., Fisher, M. E., Pells, T. J., James-Zorn, C., Wang, Y., Ponferrada, V. G., Zorn, A. M., & Vize, P. D. (2018). Xenbase: A genomic, epigenomic and transcriptomic model organism database. *Nucleic Acids Research*, *46*(D1), D861–D868. https://doi.org/10.1093/nar/gkx936

Keller, R., Davidson, L. A., & Shook, D. R. (2003). How we are shaped: The biomechanics of gastrulation. *Differentiation*, *71*(3), 171–205. https://doi.org/10.1046/j.1432-0436.2003.710301.x

Knapp, J. (2018) β-Parvin Mediates Novel Integrin Signaling Pathways During Early *Xenopus laevis* Development. *PhD Thesis. University of Waterloo.*

Kraft, B., Berger, C. D., Wallkamm, V., Steinbeisser, H., & Wedlich, D. (2012). Wnt-11 and Fz7 reduce cell adhesion in convergent extension by sequestration of PAPC and C-

cadherin. *Journal of Cell Biology*, *198*(4), 695–709. https://doi.org/10.1083/jcb.201110076

Lee, C.-H., & Gumbiner, B. M. (1995). Disruption of gastrulation movements in Xenopus by a dominant-negative mutant for C-cadherin. *Developmental Biology*, *171*(2), 363–373. https://doi.org/10.1006/dbio.1995.1288

Lee, G., Hynes, R., & Kirschner, M. (1984). Temporal and spatial regulation of fibronectin in early Xenopus development. *Cell*, *36*(3), 729–740. https://doi.org/10.1016/0092-8674(84)90353-2

Legate, K. R., Montañez, E., Kudlacek, O., & Fässler, R. (2006). ILK, PINCH and parvin: The tIPP of integrin signalling. *Nature Reviews Molecular Cell Biology*, *7*(1), 20–31. https://doi.org/10.1038/nrm1789

Leonard, M., Chan, Y., & Menko, A. S. (2008). Identification of a novel intermediate filament-linked N-cadherin/γ-catenin complex involved in the establishment of the cytoarchitecture of differentiated lens fiber cells. *Developmental Biology*, *319*(2), 298–308. https://doi.org/10.1016/j.ydbio.2008.04.036

Levi, G., Ginsberg, D., Girault, J.-M., Sabanay, I., Thiery, J. P., & Geiger, B. (1991). EP-cadherin in muscles and epithelia of Xenopus laevis embryos. *Development*, *113*(4), 1335–1344.

Lin, X., Qadota, H., Moerman, D. G., & Williams, B. D. (2003). C. elegans PAT-6/actopaxin plays a critical role in the assembly of integrin adhesion complexes in vivo. *Current Biology*, *13*(11), 922–932. https://doi.org/10.1016/S0960-9822(03)00372-5

Logan, C. Y., Miller, J. R., Ferkowicz, M. J., & McClay, D. R. (1999). Nuclear β-catenin is required to specify vegetal cell fates in the sea urchin embryo. *Development*, *126*(2), 345–357.

Marchuk, D., Drumm, M., Saulino, A., & Collins, F. S. (1991). Construction of T-vectors, a rapid and general system for direct cloning of unmodified PCR products. Nucleic Acids Research, 19(5), 1154. https://doi.org/10.1093/nar/19.5.1154

Marsden, M., & DeSimone, D. W. (2001). Regulation of cell polarity, radial intercalation and epiboly in Xenopus: Novel roles for integrin and fibronectin. *Development*, *128*(18), 3635–3647. https://doi.org/10.1242/dev.128.18.3635

Marsden, M., & DeSimone, D. W. (2003). Integrin-ECM interactions regulate cadherin-dependent cell adhesion and are required for convergent extension in Xenopus. *Current Biology*, *13*(14), 1182–1191. https://doi.org/10.1016/S0960-9822(03)00433-0

McCrea, P. D., Brieher, W. M., & Gumbiner, B. M. (1993). Induction of a secondary body axis in Xenopus by antibodies to β-catenin. *Journal of Cell Biology*, *123*(2), 477–484. https://doi.org/10.1083/jcb.123.2.477

McCrea, P. D., & Gottardi, C. J. (2016). Beyond β-catenin: Prospects for a larger catenin network in the nucleus. *Nature Reviews Molecular Cell Biology*, *17*(1), 55–64. https://doi.org/10.1038/nrm.2015.3

Muhr, J., & Ackerman, K. M. (2021). Embryology, Gastrulation. In *StatPearls*. StatPearls Publishing.

Nikolopoulos, S. N., & Turner, C. E. (2000). Actopaxin, a new focal adhesion protein that binds paxillin LD motifs and actin and regulates cell adhesion. *Journal of Cell Biology*, *151*(7), 1435–1447. https://doi.org/10.1083/jcb.151.7.1435

Olski, T. M., Noegel, A. A., & Korenbaum, E. (2001). Parvin, a 42 kDa focal adhesion protein, related to the α-actinin superfamily. *Journal of Cell Science*, *114*(3), 525–538.

Park, E. C., Cho, G.-S., Kim, G.-H., Choi, S.-C., & Han, J.-K. (2011). The involvement of Eph-Ephrin signaling in tissue separation and convergence during Xenopus gastrulation movements. *Developmental Biology*, *350*(2), 441–450. https://doi.org/10.1016/j.ydbio.2010.12.012

Pilli, B. (2012) Role of PINCH during early *Xenopus* embryogenesis. *MSc Thesis. University of Waterloo.*

Rozario, T., Dzamba, B., Weber, G. F., Davidson, L. A., & DeSimone, D. W. (2009). The physical state of fibronectin matrix differentially regulates morphogenetic movements in vivo. *Developmental Biology*, *327*(2), 386–398. https://doi.org/10.1016/j.ydbio.2008.12.025

Schneider, S., Steinbeisser, H., Warga, R. M., & Hausen, P. (1996). β-catenin translocation into nuclei demarcates the dorsalizing centers in frog and fish embryos. *Mechanisms of Development*, *57*(2), 191–198. https://doi.org/10.1016/0925-4773(96)00546-1

Sepulveda, J. L., & Wu, C. (2006). The parvins. *Cellular and Molecular Life Sciences*, *63*(1), 25–35. https://doi.org/10.1007/s00018-005-5355-1

Session, A. M., Uno, Y., Kwon, T., Chapman, J. A., Toyoda, A., Takahashi, S., Fukui, A., Hikosaka, A., Suzuki, A., Kondo, M., Taira, M., & Rokhsar, D. S. (2016). Genome evolution in the allotetraploid frog Xenopus laevis. *Nature*, *538*(7625), 336–343. https://doi.org/10.1038/nature19840

Singhal, N. (2005). The role of *Xenopus* BRG1, a conserved subunit of SWI/SNF class of remodeling complexes, during early frog development. *Dissertation. LMU München: Faculty of Biology*

Studholme, C. (2013). β-Parvin Mediates Adhesion Receptor Cross-Talk During *Xenopus laevis* Gastrulation. *PhD Thesis. University of Waterloo.*

Takada, Y., Ye, X., & Simon, S. (2007). The integrins. *Genome Biology*, *8*(5). https://doi.org/10.1186/gb-2007-8-5-215

Tu, Y., Huang, Y., Zhang, Y., Hua, Y., Wu, C., & Wu, C. (2001). A new focal adhesion protein that interacts with integrin-linked kinase and regulates cell adhesion and spreading. *Journal of Cell Biology*, *152*(3), 585–598. https://doi.org/10.1083/jcb.153.3.585

Vakaloglou, K. M., Chountala, M., & Zervas, C. G. (2012). Functional analysis of parvin and different modes of IPP-complex assembly at integrin sites during Drosophila development. *Journal of Cell Science*, *125*(13), 3221–3232. https://doi.org/10.1242/jcs.102384

Veevers-Lowe, J., Ball, S. G., Shuttleworth, A., & Kielty, C. M. (2011). Mesenchymal stem cell migration is regulated by fibronectin through a5b1-integrin-mediated activation of PDGFR-β and potentiation of growth factor signals. *Journal of Cell Science*, *124*(8), 1288–1300. https://doi.org/10.1242/jcs.076935

Wacker, S., Grimm, K., Joos, T., & Winklbauer, R. (2000). Development and control of tissue separation at gastrulation in Xenopus. *Developmental Biology*, *224*(2), 428–439. https://doi.org/10.1006/dbio.2000.9794

Wagner, R. W., Smith, J. E., Cooperman, B. S., & Nishikura, K. (1989). A double-stranded RNA unwinding activity introduces structural alterations by means of adenosine to inosine conversions in mammalian cells and Xenopus eggs. *Proceedings of the National Academy of Sciences of the United States of America*, *86*(8), 2647–2651. https://doi.org/10.1073/pnas.86.8.2647

Webb, D. J., Parsons, J. T., & Horwitz, A. F. (2002). Adhesion assembly, disassembly and turnover in migrating cells - Over and over and over again. *Nature Cell Biology*, *4*(4). https://doi.org/10.1038/ncb0402-e97

Winklbauer, R. (1998). Conditions for fibronectin fibril formation in the early Xenopus embryo. *Developmental Dynamics*, *212*(3), 335–345. https://doi.org/10.1002/(SICI)1097-0177(199807)212:3<335::AID-AJA1>3.0.CO;2-I

Winklbauer, R., & Schürfeld, M. (1999). Vegetal rotation, a new gastrulation movement involved in the internalization of the mesoderm and endoderm in Xenopus. *Development*, *126*(16), 3703–3713. https://doi.org/10.1242/dev.126.16.3703

Yasunaga, T., Kusakabe, M., Yamanaka, H., Hanafusa, H., Masuyama, N., & Nishida, E. (2005). Xenopus ILK (integrin-linked kinase) is required for morphogenetic movements during gastrulation. *Genes to Cells*, *10*(4), 369–379. https://doi.org/10.1111/j.1365-2443.2005.00841.x

Zaidel-Bar, R., & Geiger, B. (2010). The switchable integrin adhesome. *Journal of Cell Science*, *123*(9), 1385–1388. https://doi.org/10.1242/jcs.066183

Zervas, C. G., & Brown, N. H. (2002). Integrin adhesion: When is a kinase a kinase? *Current Biology*, *12*(10). https://doi.org/10.1016/S0960-9822(02)00856-4

Zervas, C. G., Psarra, E., Williams, V., Solomon, E., Vakaloglou, K. M., & Brown, N. H. (2011). A central multifunctional role of integrin-linked kinase at muscle attachment sites. *Journal of Cell Science*, *124*(8), 1316–1327. https://doi.org/10.1242/jcs.081422

Zhang, Y., Chen, K., Tu, Y., Velyvis, A., Yang, Y., Qin, J., & Wu, C. (2002). Assembly fo the PINCH-IL-CH-ILKBP complex precedes and is essential for localization of each component to cell-matrix adhesion sites. *Journal of Cell Science*, *115*(24), 4777–4786. https://doi.org/10.1242/jcs.00166

Zhang, Y., Chen, K., Tu, Y., & Wu, C. (2004). Distinct roles of two structurally closely related focal adhesion proteins, α-parvins and β-parvins, in regulation of cell morphology and survival. *Journal of Biological Chemistry*, *279*(40), 41695–41705. https://doi.org/10.1074/jbc.M401563200